THE UNIVERSITY OF MICHIGAN

7300-1-T

Radant Analysis Studies

Interim Report No. 1
30 April through 31 July 1965

August 1965

Contract No. AF 33(615)-2811

Project 4161, Task 416103

Air Force Avionics Laboratory, AVWC
Research and Technology Division, AFSC
Wright-Patterson Air Force Base, Ohio 45433

FOREWORD

This report was prepared by The University of Michigan under USAF Contract No. AF 33(615)-2811, Task 416103, Project 4161. The work was administered under the direction of the Air Force Avionics Laboratory, Research and Technology Division, Air Force Systems Command, E.M. Turner, Technical Manager; G. Tarrants, Project Engineer.

This report covers work conducted from May through July 1965.

TABLE OF CONTENTS

ABSTRACT

The transmission characteristics of an anisotropic panel formed by conducting discs are investigated theoretically in this work. The result is intended to interpret the characteristics of the loop loaded radant (radome-antenna) panel originally studied at the Air Force Avionics Laboratory. Experimental work on the impedance variation of a ferrite-loaded horn antenna in the presence of the panel and the radiation pattern of the antenna structure are also reported in this interim report.

I
INTRODUCTION

In this report we will consider a particular radant structure. It consists of a panel which contains a square array of rectangular loops. This array is illuminated by a ferrite loaded slot antenna. The characteristics of the transmission pattern are then desired.

It was reported, at the initiation of the contract work, that a significant improvement in gain and directivity as compared to a uniformly illuminated aperture was obtained with this radant structure. These initial experiments were performed at the Wright-Patterson Air Force Base Avionics Laboratory. The more significant gain improvements were obtained with the ferrite loaded slot antenna as a primary source at the low frequencies between 200-700 Mc. In this frequency range the array panel dimensions in terms of wavelength were $\frac{\lambda}{2} - \lambda$. In view of this, we will confine our analysis in this report to this frequency range. It should be pointed out that although the array panel can be termed broadband, since at these frequencies its characteristics remain fairly uniform, the radant structure, i.e. the combination of array panel and ferrite slot antenna is not. The slot antenna by itself is very frequency sensitive and its output drops sharply for frequencies not at the 350 Mc resonance. The bandwidth between half power points is 8% for the solid ferrite slot antenna alone (Adams, 1964).

It was reported that the single characteristic which makes this radant structure unusual was the critical spacing that had to be maintained between the slot antenna and the array panel. This spacing was around 1"-2". In terms of wavelength it was .1λ or less. For spacings other than these the unexpected gain improvement was not observed. This adds an additional complication to an already difficult theoretical problem. Therefore in the contract work this additional complication must be resolved. Is this gain improvement primarily due to a better match to free space which the array panel provides for a low efficiency (30%) ferrite antenna or is the array panel the contributer in the gain improvement? An a priori speculation is that it is a matching phenomena, since (i) the spacing is critical, (ii) this effect was not observed at the higher frequencies when ordinary dipoles and horn antennas were used. This question can be resolved easily experimentally by using a small dipole antenna at these frequencies and observing the transmission pattern. Some experiments along those lines are planned. At present, the experimental phase of this work is concentrated on obtaining a variety of H and E plane patterns for different slot antenna-array panel spacing.

The theoretical work is concentrated on obtaining an explanation for the behavior of the radant structure at these frequencies. This problem is approached as follows: the array panel is treated as an artificial anisotropic dielectric medium. The plane wave transmission coefficient is calculated and used to obtain the transmitted field when the anisotropic panel is illuminated by a spherical source. To

expedite solutions to the theoretical problem various approximations are made, which, it is hoped, will be accurate enough so as not to introduce errors appreciably larger than are normally obtained in the experiments.

The array elements which are rectangular loops are approximated by discs. The ϵ and μ of the artificial dielectric is then readily calculated. The approximation by discs should give accurate results since at the frequencies under considerations the array elements are in the Rayleigh region and as is well known, in this region differences between various scatterers are only second order effects. The primary effects are obtained from the induced dipole moments in the scatterer. However, as the frequency is increased the derived ϵ and μ for the panel will become less accurate but will give useable results as long as $kd < 1$, where d is the length of an array element. For the array panel $d=1.63''$, and kd will be less than one for frequencies under 1200 Mc; hence, below this frequency the artificial dielectric approach is accurate.

The field of the primary source (Adams, 1964) can be obtained from the far field beam pattern of a loaded rectangular waveguide opening out into an infinite ground plane, assuming dominant mode fields. Fig. 1.1 shows the coordinate system.

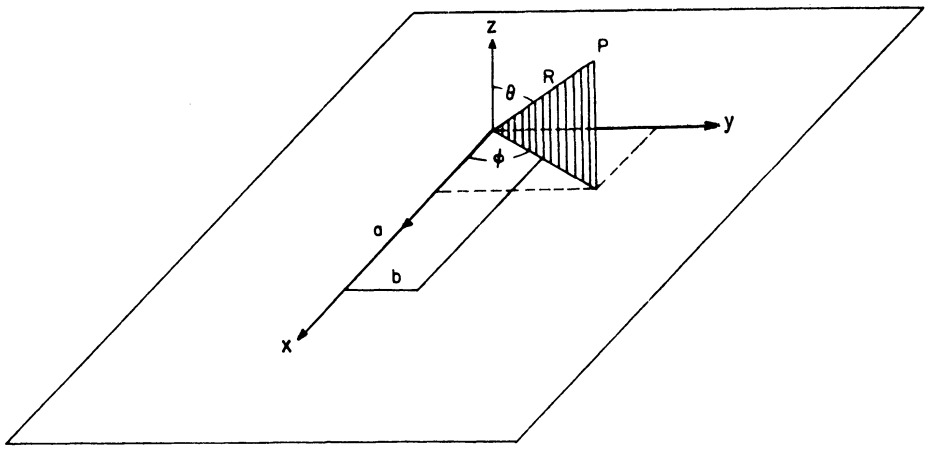

FIG. 1.1: COORDINATE SYSTEM FOR RECTANGULAR SLOT BEAM PATTERNS

The E-plane pattern $(\phi=\frac{\pi}{2})$ is

$$\underline{E}_\theta = \hat{i}_\theta E_o \frac{2}{k_o b} \frac{\sin \frac{k_o b \sin\theta}{2}}{\sin\theta} \tag{1.1}$$

and the H-plane pattern $(\phi=0)$ is

$$\underline{E}_y = \hat{i}_y E_o \frac{\pi^2 \cos\left(\frac{k_o a \sin\theta}{2}\right) \cos\theta}{\pi^2 - (k_o a \sin\theta)^2} \tag{1.2}$$

As the size of the aperture becomes electrically small, the pattern approaches that of a magnetic dipole oriented parallel to the broadwall of the waveguide $(\hat{i}_x)$.

Figure 1.2 compares experimental beam patterns of a solid ferrite loaded rectangular cavity slot antenna mounted in a 3 ft. x 3 ft. ground plane with the

corresponding theoretical patterns. Beam patterns are also shown for the same antenna without flange. It is noted that the H-plane patterns (with flange) show good agreement with the theoretical data, whereas the E-plane patterns do not. The antenna aperture was 2" by 5" (b by a). It was filled with a solid ferrite of μ=6.63, ϵ=12.6, Q=30 at 300 Mc. The resonance frequency was 350 Mc with a bandwidth of 19 Mc and efficiency of 30%.

It is seen that little agreeement between (1.1) and the experimental pattern exists. Hence in the calculations three different primary sources were used to approximate the ferrite slot antenna. The first is a tapered electric dipole oriented along the y-direction with electric field given by

$$\underline{E} = E_o \cos\theta (\hat{k} \times \hat{i}_y) \times \hat{k} \frac{e^{-jkR}}{R} \tag{1.3}$$

where $\hat{k}$ is the direction of observation. The second is a magnetic dipole oriented along the x-axis with electric field given by

$$\underline{E} = E_o (\hat{k} \times \hat{i}_x) \frac{e^{-jkR}}{R} \tag{1.4}$$

The third is a direct approximation to the experimental pattern of Fig. 1.2 with electric field in the E-plane given as

$$\underline{E} \approx E_o \cos\theta \hat{i}_\theta \frac{e^{-jkR}}{R} \tag{1.5}$$

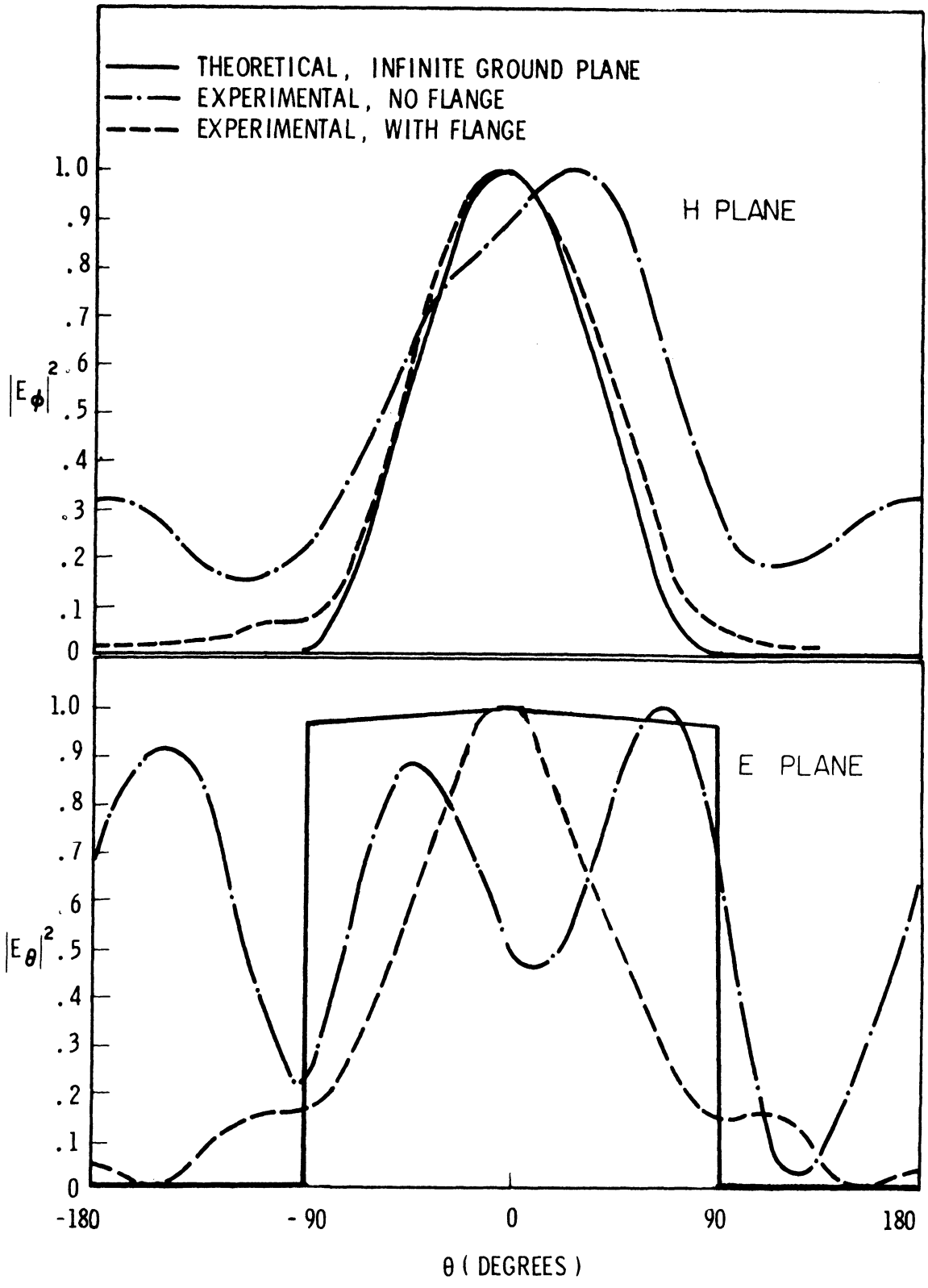

FIG. 1.2: COMPARISON OF EXPERIMENTAL AND THEORETICAL BEAM PATTERN FOR A FERRITE LOADED SLOT ANTENNA

[After Adams (1964), Fig. 27]

and the H-plane as

$$\underline{E} = E_o \cos\theta \hat{i}_y \frac{e^{-jkR}}{R} \tag{1.6}$$

II
TRANSMISSION OF PLANE ELECTROMAGNETIC WAVE THROUGH AN ARTIFICIAL ANISOTROPIC PANEL

Introduction

To give a theoretical interpretation of the transmission properties of radome structures loaded with metallic wires or loops certain models are needed. One model which may offer some useful information concerning radome structures loaded with loops is an artificial anisotropic medium made of arrays of conducting disks as shown in Fig. 2.1.

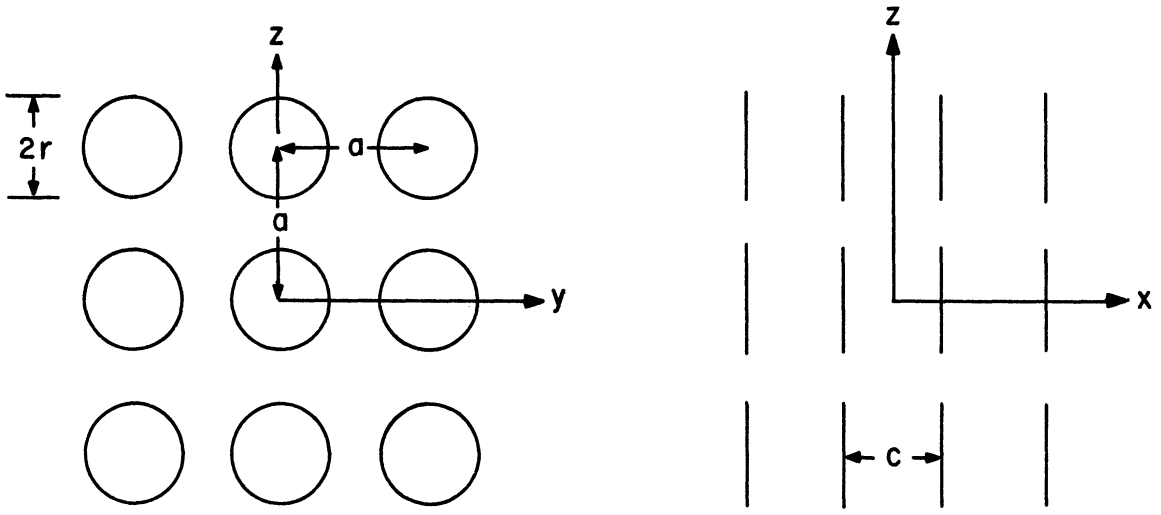

FIG. 2.1: A THREE-DIMENSIONAL ARRAY OF DISKS AS AN ARTIFICIAL ANISOTROPIC MEDIUM

Physically, the electric and the magnetic polarizability of a disk should not differ too much from that of a wire loop. Analytically, the characteristics of an artificial anisotropic medium made of disks are well known as compared with that of a loop. In this report, we shall present a theoretical analysis of the transmission property of a panel characterized by such an anisotropy.

The Tensor Permittivity and Permeability of Arrays of Disks

The tensor permittivity and permeability of a dielectric medium embedded with small conducting disks as shown in Fig. 2.1 can be determined from Rayleigh's theory of scattering by small bodies. For bodies of the shape of an oblate spheroid, the theory was reviewed in great detail by this author using the method of spheroidal harmonics (C.T. Tai, 1952). The interaction between the neighboring bodies was discussed very thoroughly by Collin (1960) who also tabulated the pertinent data for prolate spheroids, ellipsoids as well as for the oblate spheroids.

According to Rayleigh's theory, the induced electric dipole moment of an isolated disk due to an incident E-field polarized in the y or z direction can be written in the form

$$p_y = p_z = \alpha \epsilon E_o \tag{2.1}$$

where

E_o = amplitude of the incident E-field

ϵ = dielectric constant of the ambient medium

α = electric polarizability of an isolated disk = $\frac{16}{3} r^3$

r = radius of the disk

The induced magnetic dipole moment due to an incident H-field polarized in the x-direction is given by

$$m_x = \beta H_o \tag{2.2}$$

where

H_o = amplitude of the incident H-field

β = magnetic polarizability of an isolated disc

$= -\frac{8}{3} r^3$

For a three-dimensional array of disks as shown in Fig. 2.1, one must take into consideration the interaction between the disks. The resultant effective permittivity and permeability can be written in the tensor form:

$$\overline{\overline{\epsilon}} = \begin{bmatrix} \epsilon & 0 & 0 \\ 0 & \epsilon_1 & 0 \\ 0 & 0 & \epsilon_1 \end{bmatrix} \tag{2.3}$$

$$\bar{\bar{\mu}} = \begin{bmatrix} \mu_1 & 0 & 0 \\ 0 & \mu_o & 0 \\ 0 & 0 & \mu_o \end{bmatrix} \tag{2.4}$$

where

$$\epsilon_1 = K_e \epsilon = (1 + \frac{N\alpha}{1-\alpha C_e}) \epsilon \tag{2.5}$$

$$\mu_1 = K_m \mu_o = (1 + \frac{N\beta}{1-\beta C_m}) \mu_o \tag{2.6}$$

N = number of disks per unit volume
$= (a^2 c)^{-1}$

The values of the interaction constants C_e and C_m contained in (2.5) and (2.6) depend on the actual dimensionality of the lattice. There are several alternative methods of evaluating these constants as described by Collin (1960). For a cubic lattice, corresponding to a=c, the values of C_e and C_m is given quite accurately by Lorentz's formula, namely,

$$C = \frac{1}{3a^3} \quad . \tag{2.7}$$

Therefore, K_e and K_m are given, respectively, by

$$K_e = 1 + \frac{\frac{16}{3}(\frac{r}{a})^3}{1 - \frac{16}{9}(\frac{r}{a})^3} = \frac{1 + \frac{32}{9}(\frac{r}{a})^3}{1 - \frac{16}{9}(\frac{r}{a})^3} \tag{2.8}$$

and

$$K_m = 1 - \frac{\frac{8}{3}(\frac{r}{a})^3}{1+\frac{8}{9}(\frac{r}{a})^3} = \frac{1-\frac{16}{9}(\frac{r}{a})^3}{1+\frac{8}{9}(\frac{r}{a})^3} \tag{2.9}$$

Transmission of a Plane Electromagnetic Wave Through an Anisotropic Panel

Case A Incident E-field perpendicular to the plane of incidence.

We consider now the problem illustrated in Fig. 2.2 .

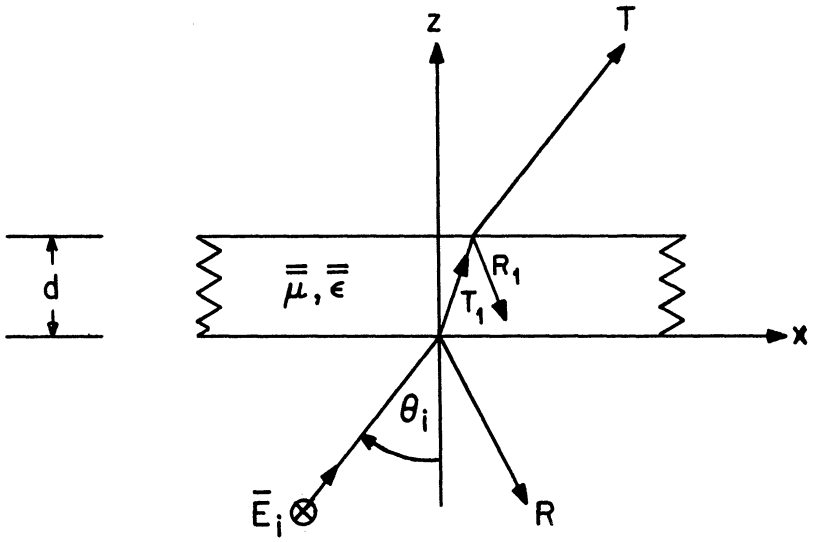

FIG. 2.2: A PLANE ELECTROMAGNETIC WAVE INCIDENT ON AN ANISOTROPIC PANEL

The tensor permittivity and permeability of the panel are the same as the ones defined by (2.3) and (2.4). The E-field of the incident plane wave is assumed to be polarized in the y-direction. The general expressions for the fields in the three regions are given by:

Region I, $z \leq 0$

$$\bar{E}^i = E_o \hat{y}\, e^{-j(k_x x + k_z z)} \tag{2.10}$$

$$\bar{H}^i = \frac{E_o}{\omega\mu_o}(-k_z x + k_x z)\, e^{-j(k_x x + k_z z)} \tag{2.11}$$

$$k_x = k_o \sin\theta_i, \quad k_z = k_o \cos\theta_i, \quad k_o = \frac{2\pi}{\lambda}$$

$$\bar{E}^r = R E_o \hat{y}\, e^{-j(k_x x - k_z z)} \tag{2.12}$$

$$\bar{H}^r = \frac{R E_o}{\omega\mu_o}(k_z \hat{x} + k_x \hat{z})\, e^{-j(k_x x - k_z z)} \tag{2.13}$$

Region II, $0 \leq z \leq d$

$$\bar{E}^d = E_o \hat{y}\left[T_1 e^{-j(k'_x x + k'_z z)} + R_1 e^{-j(k'_x x - k'_z z)}\right] \tag{2.14}$$

$$\bar{H}^d = \frac{E_o}{\omega}\left[\bar{\bar{\mu}}\right]^{-1} \cdot \left[T_1(-k'_z \hat{x} + k'_x \hat{z}) e^{-j(k'_x x - k'_z z)} + R_1(k'_z \hat{x} + k'_x \hat{z})\, e^{-j(k'_x x - k'_z z)}\right] \tag{2.15}$$

where $\left[\bar{\bar{\mu}}\right]^{-1}$ denotes the inverse of $\bar{\bar{\mu}}$, and

$$k'_x = k_x = k_o \sin\theta_i \tag{2.16}$$

$$k_z'^2 = \omega^2 \mu_1 \epsilon_1 - \left(\frac{\mu_1}{\mu_o}\right) k_x'^2$$

$$= k_o^2 K_m (K_e' - \sin^2\theta_i) \qquad (2.17)$$

$$K_e' = \frac{\epsilon}{\epsilon_o} K_e \qquad (2.18)$$

Equation (2.16) results from the boundary condition that the field inside the panel should have the same phase as the incident field at the interface in order to satisfy the boundary condition. Equation (2.17) is a consequence of the fact that any plane wave solution inside the anisotropic panel must be a solution of the wave equation:

$$\nabla \times \left[\overline{\overline{\mu}}^{-1} \cdot \nabla \times \bar{E}\right] - \omega^2 \overline{\overline{\epsilon}} \cdot \bar{E} = 0 \ .$$

Region III, $d \leq z$

$$\bar{E}^t = T E_o \hat{y}\, e^{-j(k_x x + k_z z)} \qquad (2.19)$$

$$\bar{H}^t = \frac{T E_o}{\omega \mu_o} (-k_z \hat{x} + k_x \hat{y}) e^{-j(k_x x + k_z z)} \ . \qquad (2.20)$$

By matching the tangential components of the E and H fields at the two interfaces, corresponding to z=0 and z=d, one can determine the unknown coefficients T_1, R_1, T, and R. The results are summarized below:

$$T_1 = \frac{(1+r)}{1-r^2 e^{-j2k'_z d}} \tag{2.21}$$

$$R_1 = \frac{-r(1+r)e^{-2jk'_z d}}{1-r^2 e^{-j2k'_z d}} \tag{2.22}$$

$$T = \frac{(1-r^2)e^{j(k_z - k'_z)d}}{1-r^2 e^{-j\,2k'_z d}} \tag{2.23}$$

$$R = \frac{r(1-e^{-j2k'_z d})}{1-r^2 e^{-j2k'_z d}} \tag{2.24}$$

where

$$r = \frac{(\frac{\mu_1 k_z}{\mu_o k'_z}) - 1}{(\frac{\mu_1 k_z}{\mu_o k'_z}) + 1} = \frac{Z' - Z}{Z' + Z} \tag{2.25}$$

$$Z = \frac{\omega\mu_o}{k_z} = \frac{\eta_o}{\cos\theta_i} \tag{2.26}$$

$$Z' = \frac{\omega\mu_1}{k'_z} = \frac{\eta_o\sqrt{K_m}}{\sqrt{K'_e - \sin^2\theta_i}} \tag{2.27}$$

or

$$r = \frac{\sqrt{K_m}\cos\theta_i - \sqrt{K'_e - \sin^2\theta_i}}{\sqrt{K_m}\cos\theta_i + \sqrt{K'_e - \sin^2\theta_i}} \quad . \tag{2.28}$$

It can easily be verified that

$$|T|^2 = \frac{1}{1+\left(\frac{2r\sin k'_z d}{1-r^2}\right)^2} \tag{2.29}$$

and

$$1 - |R|^2 = |T|^2 = \left(\frac{1-r}{1+r}\right)\left(|T_1|^2 - |R_1|^2\right) . \tag{2.30}$$

The power transmission coefficient $|T|^2$ becomes unity when $k'_z d$ is equal to an integral multiple of π. It is seen that for an isotropic dielectric panel the coefficient r as defined by (2.28) reduces

$$r = \frac{\cos\theta_i - \sqrt{n^2 - \sin^2\theta_i}}{\cos\theta_i + \sqrt{n^2 - \sin^2\theta_i}} \tag{2.31}$$

and the phase constant k'_z defined by (2.17) reduces to

$$k'^2_z = k_o^2 (n^2 - \sin^2\theta_i) \tag{2.32}$$

where

$$n^2 = \frac{\epsilon}{\epsilon_o} \quad . \tag{2.33}$$

These results are well known.

Case B Incident E-field parallel to the plane of incidence

The orientation of the incident wave with respect to the panel for this case is shown in Fig. 2.3.

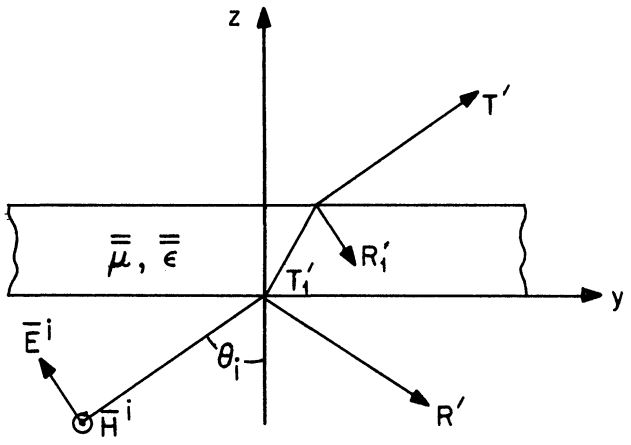

FIG. 2.3:

The tensor permittivity and permeability of the panel are the same as the ones defined by (2.3) and (2.4). It is convenient to define the reflection and the transmission coefficients with reference to the incident magnetic field. Thus, the expressions for the electromagnetic field in the different regions are given by

Region I, $z \leq 0$

$$\bar{H}^i = H_o \hat{x}\, e^{-j(\beta_y y + \beta_z z)} \tag{2.34}$$

$$\bar{E}^i = \frac{H_o}{\omega \epsilon_o} (-\beta_z \hat{y} + \beta_y \hat{z})\, e^{-j(\beta_y y + \beta_z z)} \tag{2.35}$$

where

$$\beta_y = k_o \sin\theta_i , \qquad \beta_z = k_o \cos\theta_i$$

$$k_o = \frac{2\pi}{\lambda}$$

Region II, $0 \leq z \leq d$

$$\bar{H}^d = H_o \hat{x} \left[T_1' e^{-j(\beta_y' y + \beta_z' z)} + R_1' e^{-j(\beta_y' y - \beta_z' z)} \right] \tag{2.36}$$

$$\bar{E}^d = \frac{H_o}{\omega} \left[\bar{\bar{\epsilon}}\right]^{-1} \cdot \left[T_1' (-\beta_z' y + \beta_y' z) e^{-j(\beta_y' y + \beta_z' z)} + R_1' (\beta_z' y + \beta_y' z)\, e^{-j(\beta_y' y - \beta_z' z)} \right] \tag{2.37}$$

where $\left[\bar{\bar{\epsilon}}\right]^{-1}$ denotes the inverse of $\bar{\bar{\epsilon}}$, and

$$\beta_y' = \beta_y = k_o \sin\theta_i$$

$$\beta_z'^2 = \omega^2 \mu_1 \epsilon_1 - \beta_y'^2$$

$$= k_o^2 (K_m K_e' - \sin^2\theta_i)$$

$$K_e' = \frac{\epsilon}{\epsilon_o} K_e$$

Region III, $d \leq z$

$$\bar{H}^t = T' H_o \hat{x}\, e^{-j(\beta_y y + \beta_z z)} \tag{2.38}$$

$$\bar{E}^t = \frac{T' H_o}{\omega \epsilon_o} (-\beta_z \hat{y} + \beta_y \hat{z}) e^{-j(\beta_y y + \beta_z z)} \tag{2.39}$$

By matching the tangential components of the E and H fields at the two interfaces, corresponding to z=0 and z=d, one can determine the unknown coefficients T'_1, R'_1, T' and R'. The results have the same algebraic forms as those given by (21) to (24) except that the coefficients k_z, k'_z and r are replaced, respectively, by β_z, β'_z and r' which are defined by

$$\beta_z = k_o \cos\theta_i \tag{2.40}$$

$$\beta'_z = k_o \sqrt{K_m K'_e - \sin^2\theta_i} \tag{2.41}$$

$$r' = \frac{K'_e \cos\theta_i - \sqrt{K_m K'_e - \sin^2\theta_i}}{K'_e \cos\theta_i + \sqrt{K_m K'_e - \sin^2\theta_i}} \tag{2.42}$$

Thus, the expression for $|T'|^2$ is given by

$$|T'|^2 = \frac{1}{1+\left(\dfrac{2r' \sin\beta'_z d}{1-r'^2}\right)^2} \tag{2.43}$$

Numerical Computation and Conclusion

Before we discuss the effect of loading it is of some interest to point out the special characteristics of transparent panels at oblique incidence. Referring to Eqs. (2.29) and (2.43) we see that $|T|^2$ becomes unity when

$$k_o d \sqrt{K_m (K'_e - \sin^2 \theta_i)} = N\pi \tag{2.44}$$

and $\left| T' \right|^2$ becomes unity when

$$k_o d \sqrt{K_m K'_e - \sin^2 \theta_i} = N'\pi \tag{2.45}$$

where N and N' denote two integers. If we use the notations "$\perp$" and "$//$" to distinguish the two cases then the respective angle of incidences at which the power transmission coefficient becomes unity are given by

$$\sin^2 (\theta_i)_\perp = K'_e - \frac{1}{K_m} \left(\frac{N\lambda}{2d} \right)^2 \tag{2.46}$$

and

$$\sin^2 (\theta_i)_{//} = K_m K'_e - \left(\frac{N'\lambda}{2d} \right)^2 \tag{2.47}$$

For convenience, these angles will be designated as "angle of transparency". For a panel with given values of K'_e and K_m it is possible to find the values for d such that the angle of transparency may occur at any desirable angle of incidence. For example, when $\frac{d}{\lambda} = \frac{1}{2}$ $K_m = 1$, $K'_e = 2$, $(\theta_i)_\perp$ or $(\theta_i)_{//}$ occurs at $\pi/2$. The curve labeled $\frac{d}{\lambda} = \frac{1}{2}$ in Fig. 1 shows such a case. In general, the transmission coefficient approaches zero when θ_i approaches 90^o, corresponding to the grazing incidence, unless the thickness of the panel is such that the angle of transparency occurs at the grazing incidence.

When the incident E-field is perpendicular to the plane of incidence, it is seen from Fig. 2.1 and Fig. 2.4 that for a panel with relative permittivity equal to two, the effect of disc loading, in general, does not change much the transmission characteristics except when the panel is transparent at certain incident angle, corresponding to $d/\lambda=0.379$ in Fig. 2.4. For a denser panel, the loading may change considerably the angular dependence as shown by Figs. 2.5 and 2.8. In fact, for a panel with a thickness between a quarter-wavelength and a half-wavelength, the loading tends to provide a more uniform transmission except near the grazing incidence.

When the incident E-field is parallel to the plane of incidence a dielectric panel becomes transparent when the angle of incidence is equal to the Brewster angle given by

$$(\theta_i) = \tan^{-1}\sqrt{\frac{\epsilon}{\epsilon_o}} \tag{2.48}$$

For $\frac{\epsilon}{\epsilon_o}=2$ and 4, the Brewster angle occurs, respectively, at 54^o-44' and 63^o-26" as shown in Figs. 2.9 and 2.10.

For a panel made of discs only, the power transmission coefficient, as shown in Fig. 2.11, is not too sensitive with respect to the thickness of the panel. The effect of disc loading in a dielectric panel is similar to the previous case. However, because of the phenomenon of transparency at the Brewster angle, the transmission coefficient tends to be more uniform with respect to the incident

angle, unless the dielectric constant of the panel is high to start with, as shown by Fig. 2.13. By choosing the lattice spacing properly such that $K_m K'_e = 1$, it is theoretically possible to move the Brewster angle to the grazing direction, hence to provide a quite uniform transmission through the panel.

It is hoped that the study presented here may be used later to interpret the radiation pattern of a loop-radome structure which is presently being investigated experimentally.

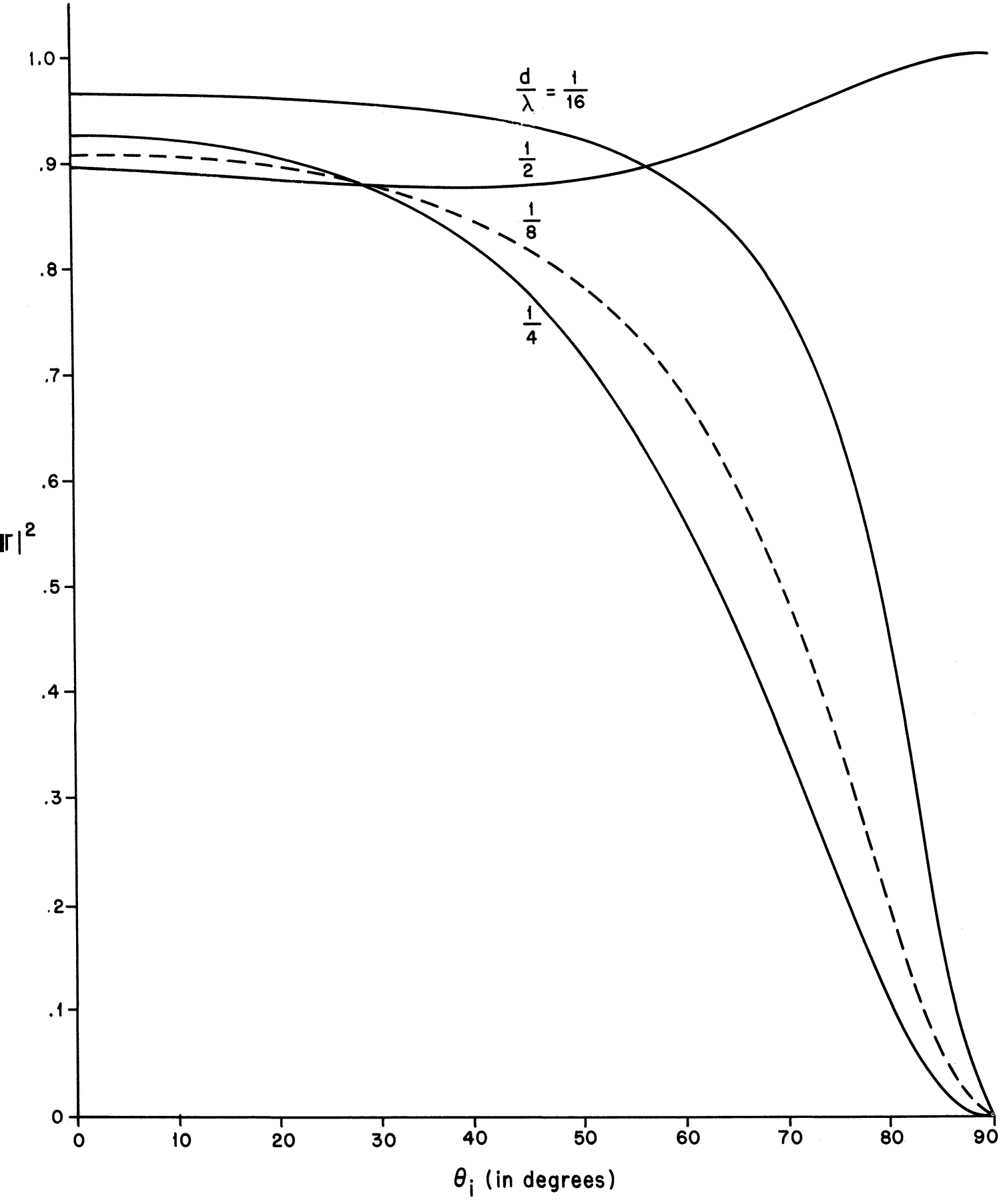

FIG. 2.4: THE TRANSMISSION COEFFICIENT $|T|^2$ FOR $K_m=1$, $K_e=1$, $\frac{\epsilon}{\epsilon_o}=2$

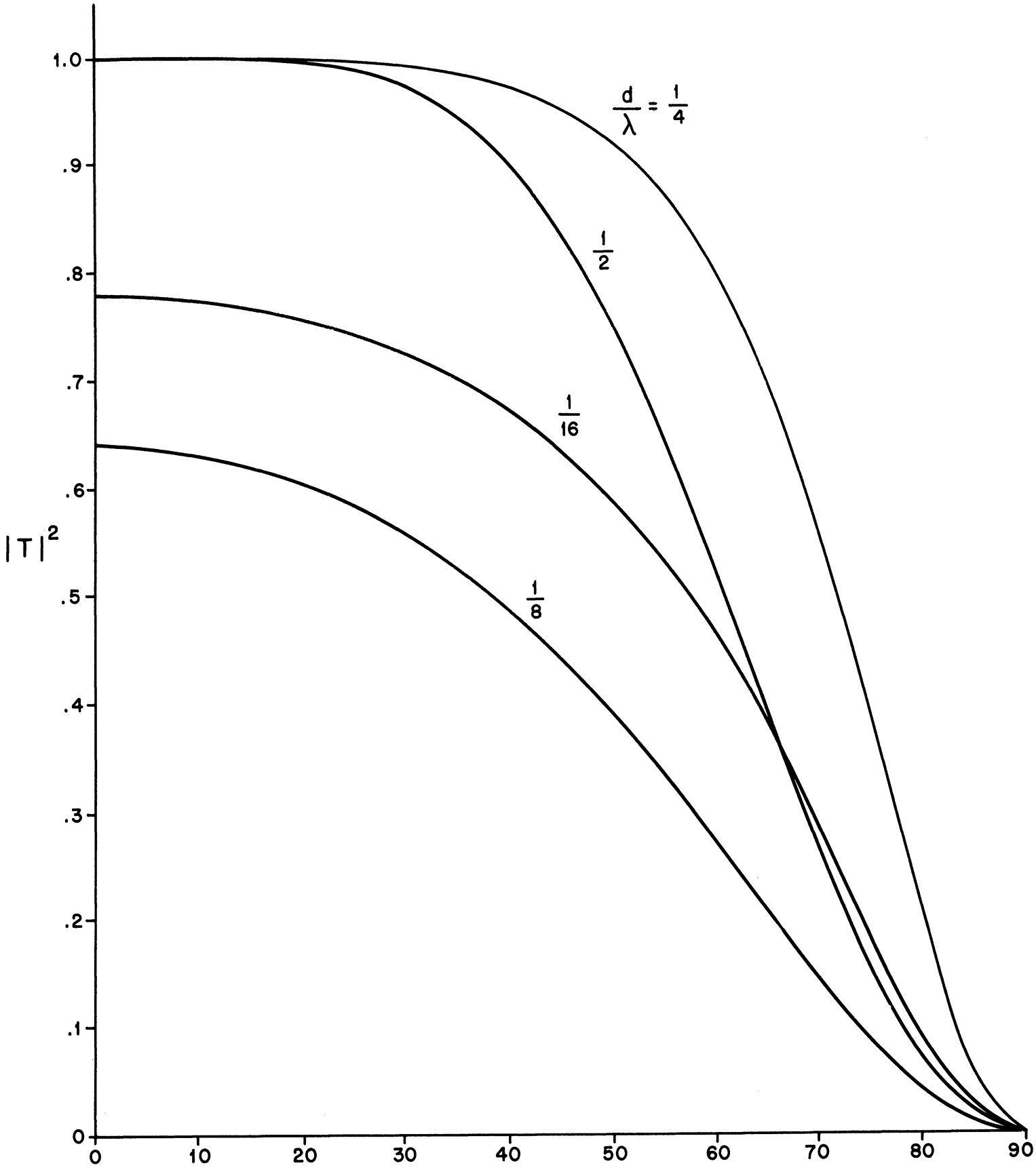

FIG. 2.5: THE TRANSMISSION COEFFICIENT $|T|^2$ FOR $K_m=1$, $K_e=1$, $\frac{\epsilon}{\epsilon_o} = 4$

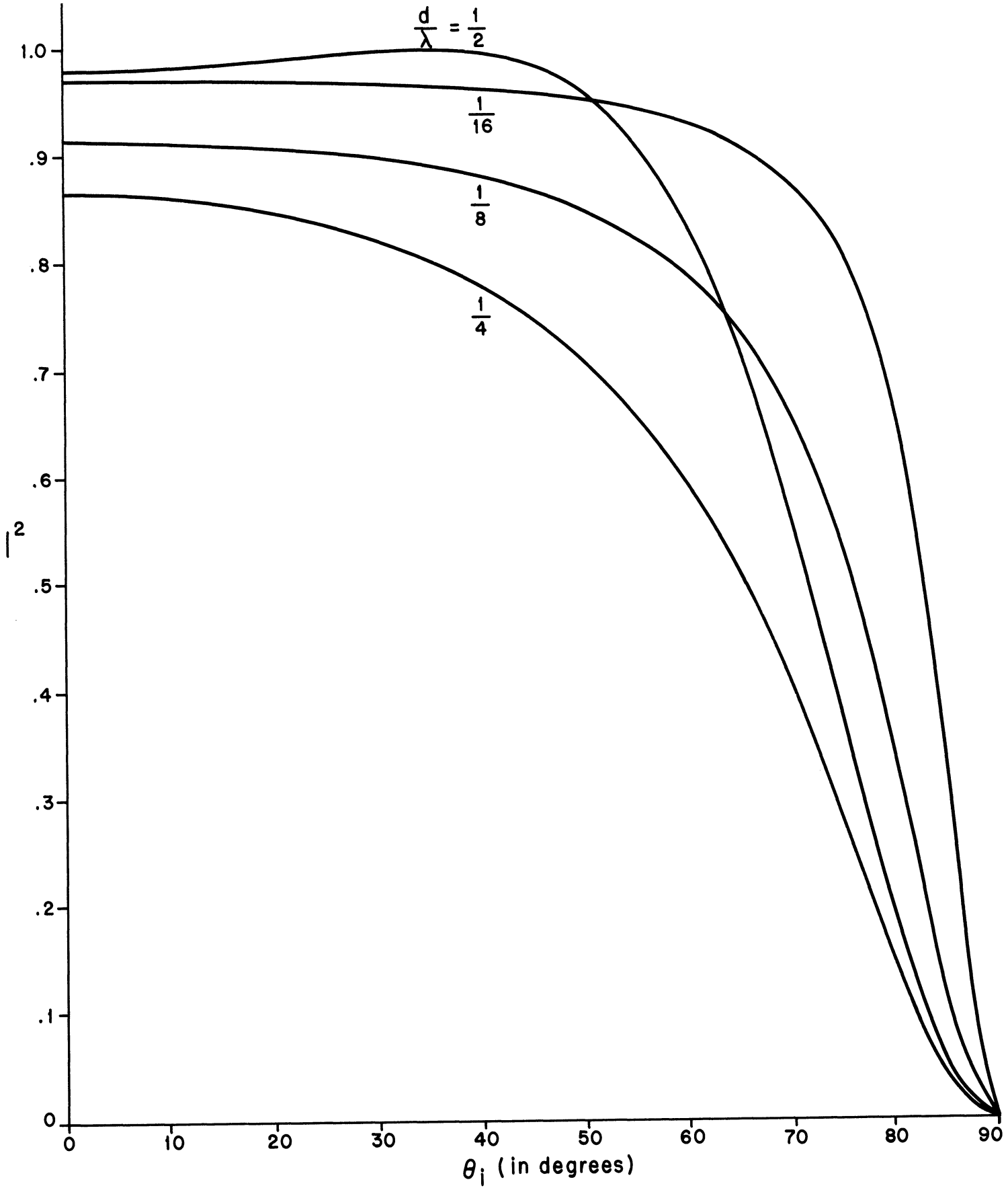

FIG. 2.6: THE TRANSMISSION COEFFICIENT $|T|^2$ FOR K_m=0.755, K_e=1.65, $\frac{\epsilon}{\epsilon_o} = 1$

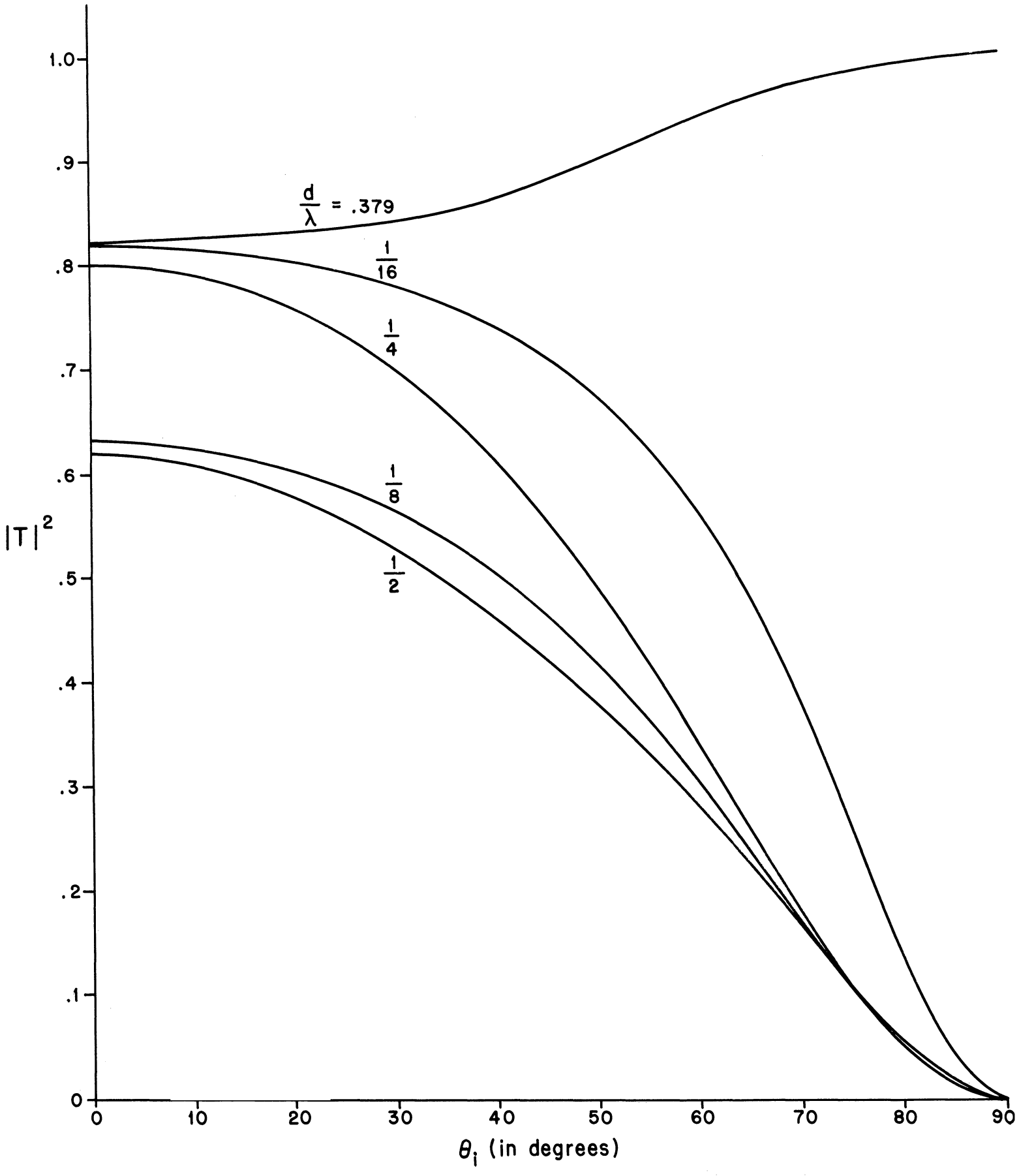

FIG. 2.7: THE TRANSMISSION COEFFICIENT $|T|^2$ FOR $K_m = 0.755$, $K_e = 1.65$, $\frac{\epsilon}{\epsilon_o} = 2$

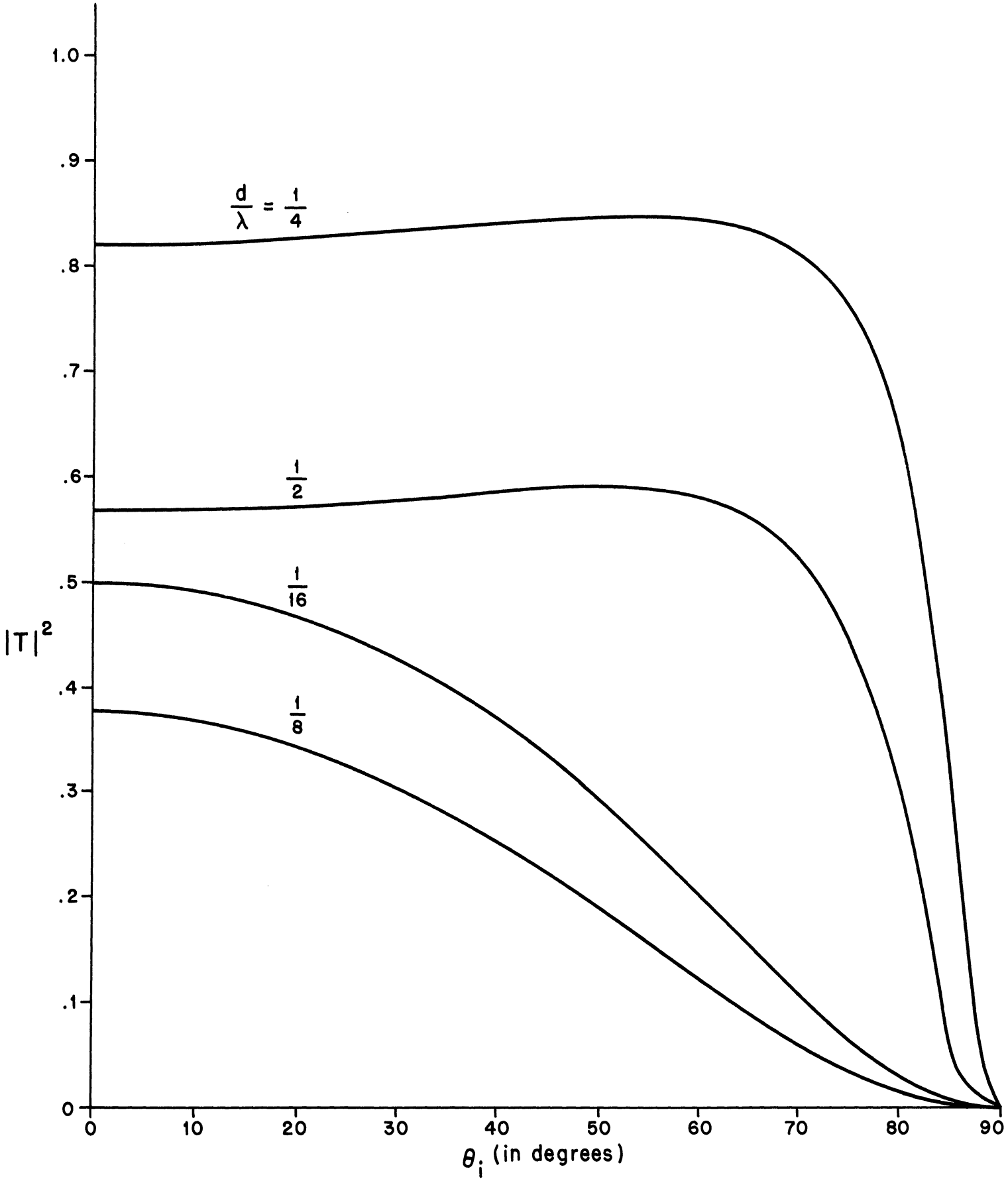

FIG. 2.8: THE TRANSMISSION COEFFICIENT $|T|^2$ FOR K_m=0.755, K_e=1.65, $\frac{\epsilon}{\epsilon_o} = 4$

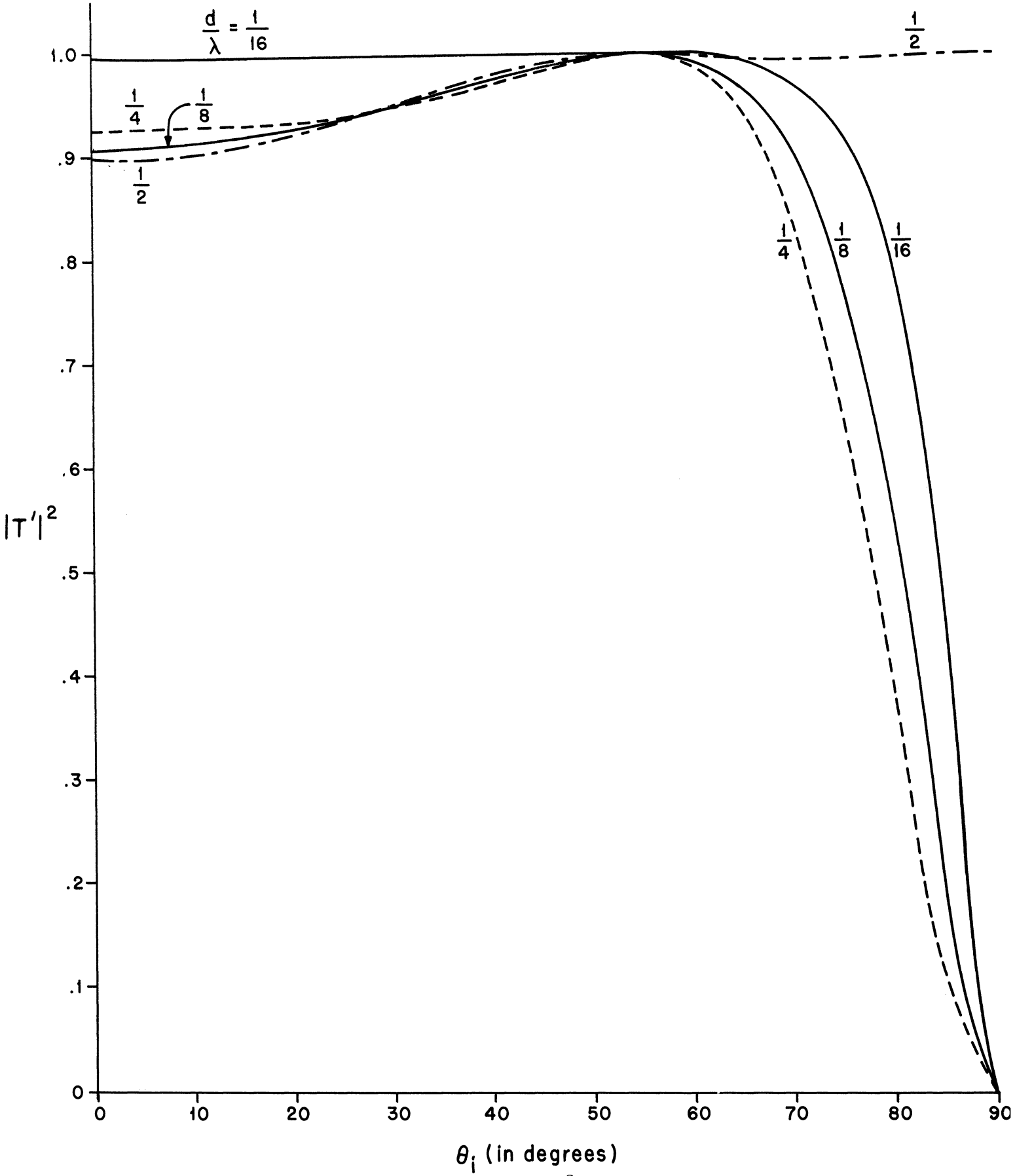

FIG. 2.9: THE TRANSMISSION COEFFICIENT $\left|T'\right|^2$ FOR $K_m=1$, $K_e=1$, $\frac{\epsilon}{\epsilon_o}=2$

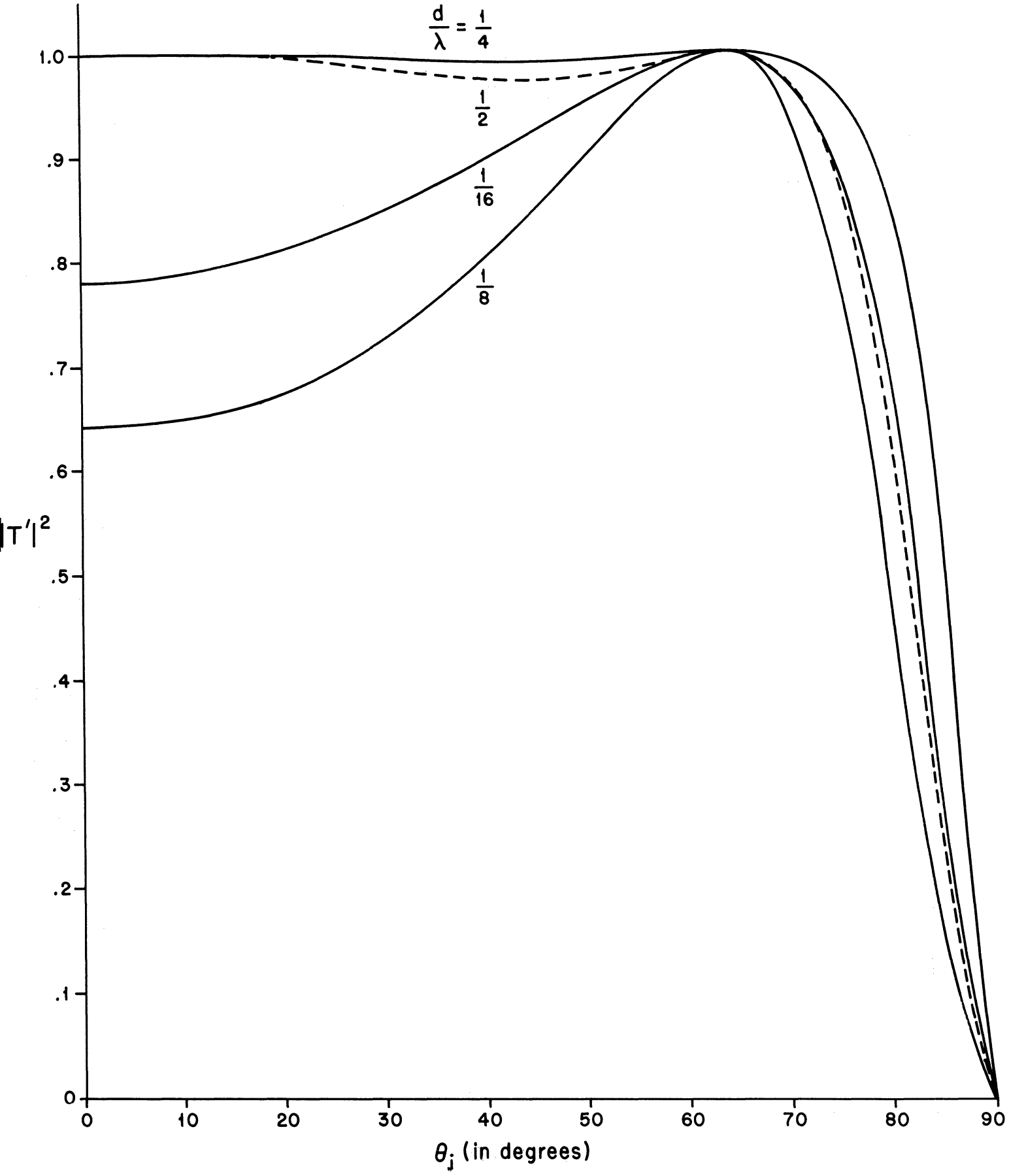

FIG. 2.10: THE TRANSMISSION COEFFICIENT $|T'|^2$ FOR $K_m=1$, $K_e=1$, $\frac{\epsilon}{\epsilon_o}=4$

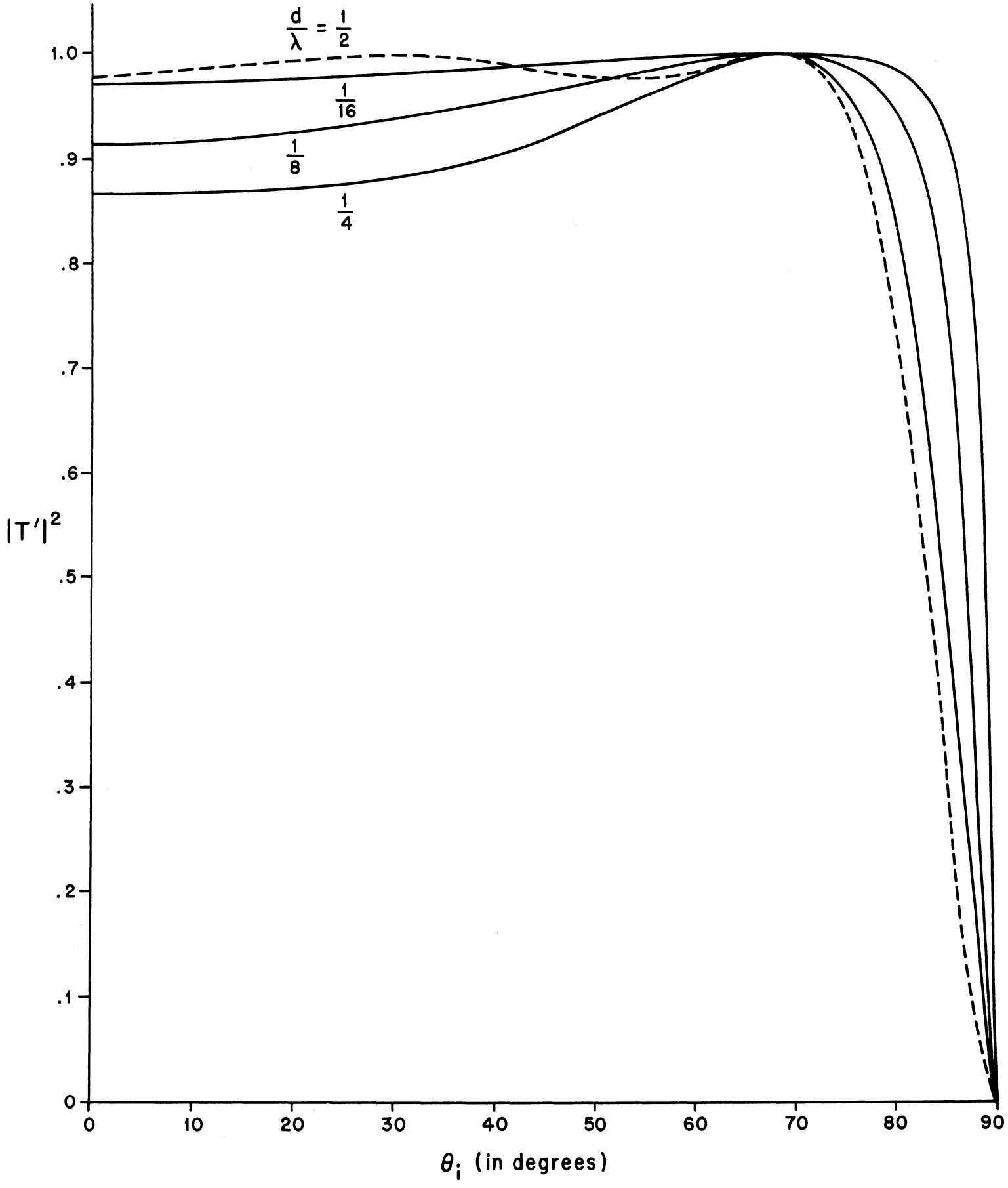

FIG. 2.11: THE TRANSMISSION COEFFICIENT $|T'|^2$ FOR K_m=0.755, K_e=1.65, $\frac{\epsilon}{\epsilon_o} = 1$

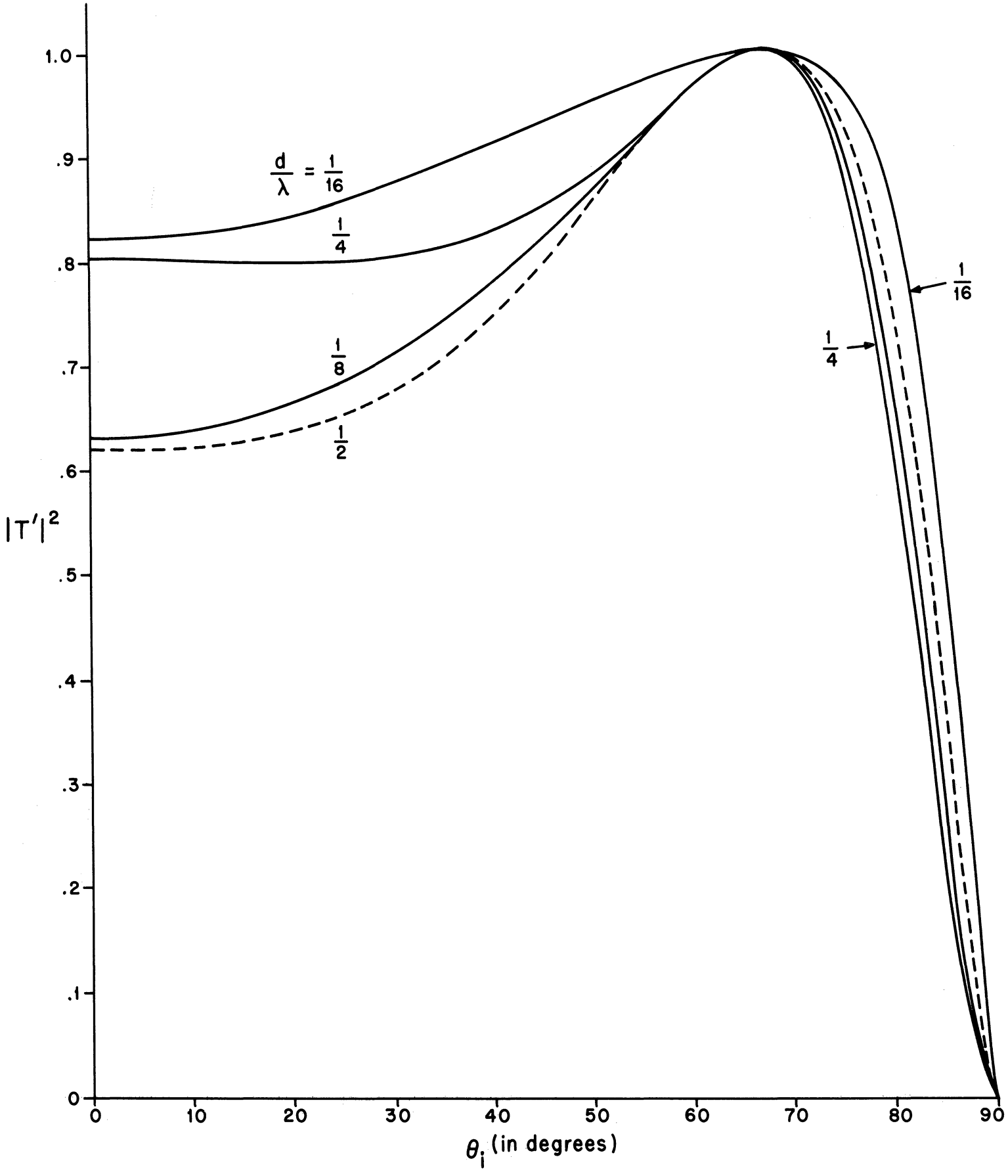

FIG. 2.12: THE TRANSMISSION COEFFICIENT $|T'|^2$ FOR K_m=0.755, K_e=1.65, $\frac{\epsilon}{\epsilon_o} = 2$

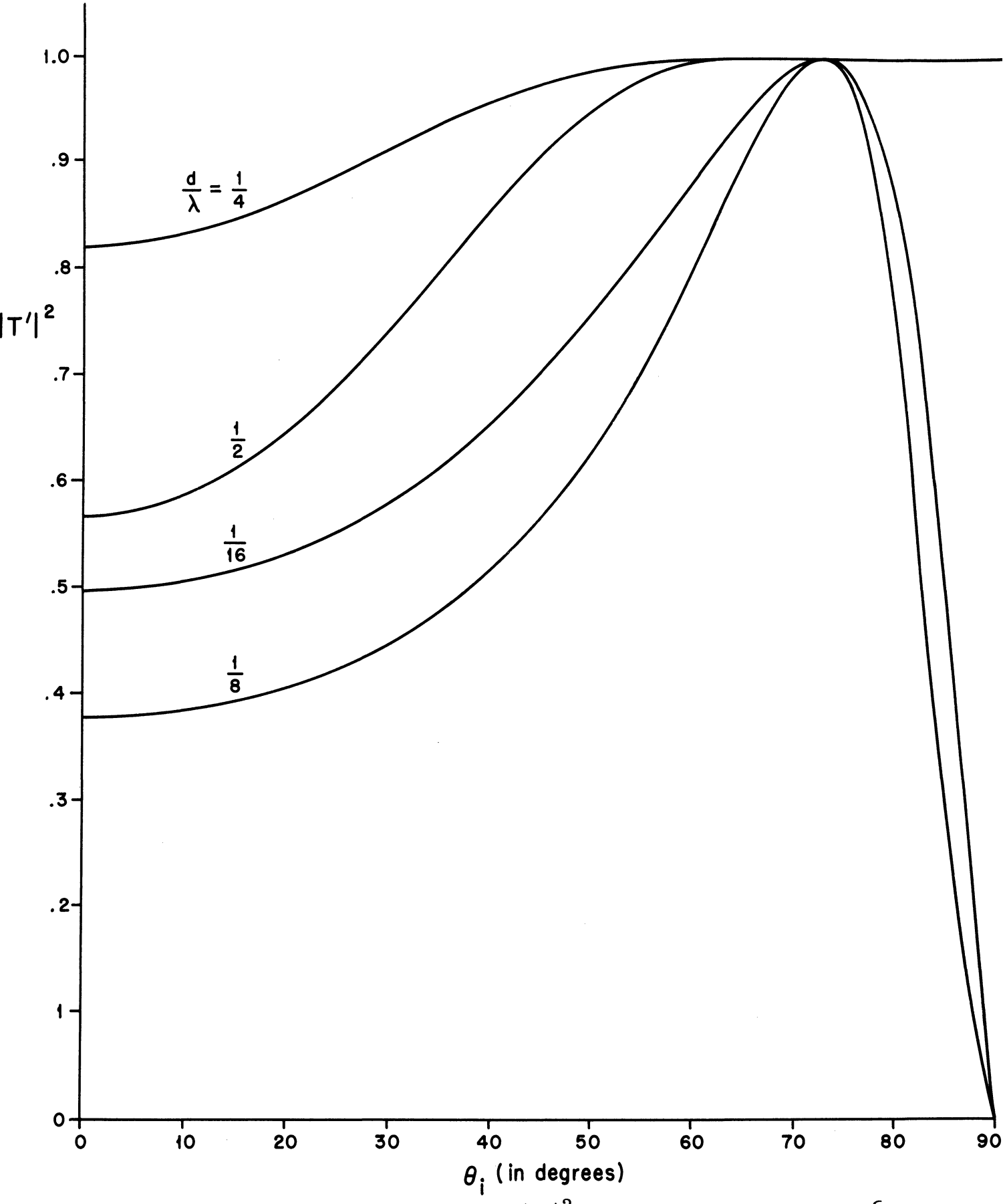

FIG. 2.13: THE TRANSMISSION COEFFICIENT $|T'|^2$ FOR K_m=0.755, K_e=1.65, $\frac{\epsilon}{\epsilon_o} = 4$

III
TRANSMISSION PATTERNS OF AN ANISOTROPIC PANEL EXCITED BY A SPHERICAL SOURCE

Introduction and Formulation

We would like to obtain the field pattern which an anisotropic dielectric panel transmitts when excited by a small electromagnetic horn. The panel is an array of loops or discs which can be treated as an artificial anisotropic medium for which the tensor permittivity and permeability is found elsewhere. The plane wave transmis sion coefficient T for a panel of thickness d can then be obtained by the usual method of matching the tangential fields at the two surfaces of the panel. The excitation will be a horn or dipole antenna placed in the near or far field of the panel. To use the plane wave transmission coefficient when the source emmits spherical waves is very difficult. However, by assuming a cylindrical wavefront, the plane wave transmission coefficient can be readily used. Assuming a cylindrical wave, corresponds to a one-dimens ional analysis for our panel. This should give negligible error if we confine ourselves to E-plane and H-plane transmitted fields.

Looking at a continuous one-dimensional radiating source, as shown in Fig. 3.1, the far field can be expressed as

$$E(r,\theta) = \int_{-a}^{a} f(x') \frac{e^{-jk_o R}}{R} dx' \approx \frac{e^{-jk_o r}}{r} \int_{-a}^{a} f(x') e^{jk_o x' \sin\theta} dx' \qquad (3.1)$$

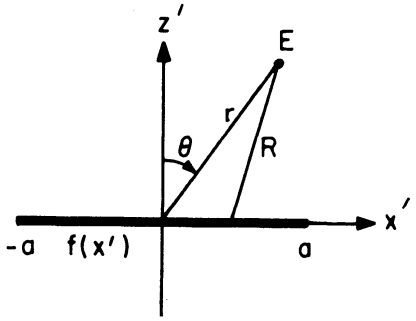

FIG. 3.1: A RADIATING CONTINUOUS SOURCE

However, when the panel is not a radiator itself, but is excited by a remote source, it should be treated as a secondary source. The reason for this is that the source will not only excite the panel but also the extension of the panel area which is free space. This extension will contribute to the observation point $E(r,\theta)$ in a Huygens source sense, i.e. the free space extension can be considered as a secondary source made of Huygens wavelets.

Let us consider the special case of a plane boundary surface S_1. For a plane infinite surface it can be shown, either by Babinet's principle or symmetry considerations that the equivalent electric and magnetic sources $n \times \underline{H}$ and $n \times \underline{E}$ contribute equally. Hence, the scattered field can be obtained from one of these terms alone, simply by doubling it. Applying the vector Huygens-Kirchhoff formula to this case we obtain the field $\underline{E}(\underline{r})$ in terms of an integral over the plane surface S_1

$$\underline{E}(\underline{r}) = 2\nabla \times \iint_{S_1} \hat{n} \times \underline{E}(\rho') \, G(\underline{r}, \underline{\rho}') da' \qquad (3.2)$$

where $G = \frac{1}{4\pi} \frac{e^{-jkR}}{R}$; the radiation condition was applied to make the surface integral vanish at infinity. This is an exact form and is particularly suitable when apertures in a perfectly conducting screen are considered. Equation (3.2) is exact if the correct tangential component of $\underline{E}$ over the apertures are inserted.

To apply (3.2) when the surface S_1 is a combination of free space and a dielectric panel, we can let the aperture in a perfectly conducting plane sheet become very large and consider this large aperture to be the combination of free-space and the dielectric panel. Hence (3.2) is also valid for a plane dielectric surface of infinite extent. The geometry is shown in Fig. 3.2.

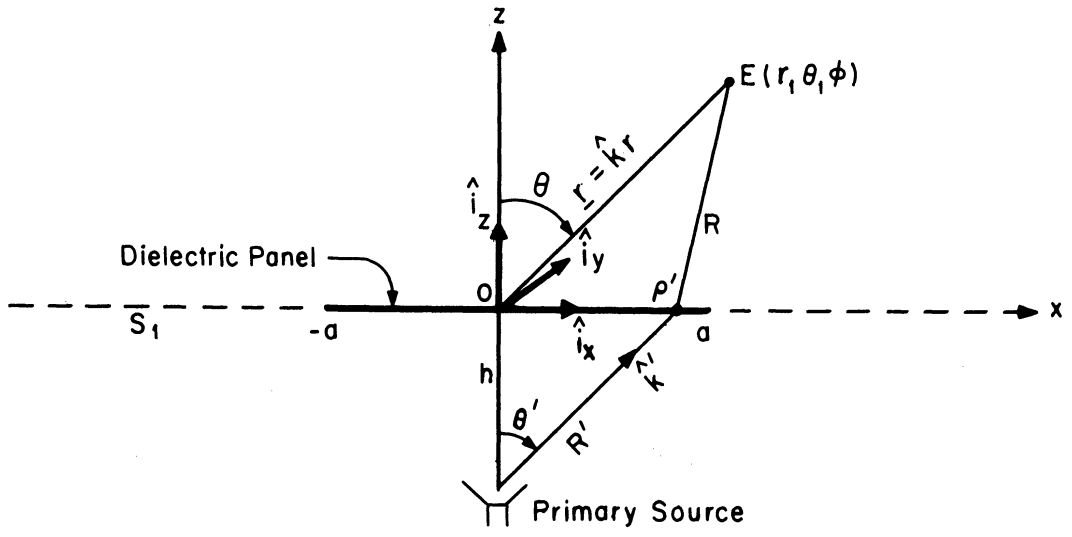

FIG. 3.2: GEOMETRY OF THE DIELECTRIC PANEL

The primary source will be a small electromagnetic horn or a small dipole which will be placed in the near field or the far field of the plate. Let us approximate the primary source by a dipole source oriented along the y-direction with an additional $\cos\theta'$ tapering as

$$\underline{E}_{horn} = E_o \cos\theta' (\hat{k}' \times \hat{i}_y) \times \hat{k}' \frac{e^{-jk_o R'}}{R'} \tag{3.3}$$

As we pointed out before we would like to use a plane wave transmission coefficient when a portion of S_1 is a plane dielectric panel. The particular form (3) assumed for the primary source will make this difficult unless we use a matrix representation for T. Since the plane wave transmission coefficients, one for perpendicular and one for parallel polarization, are relatively easily derived for a dielectric panel, we will facilitate their use by assuming a cylindrical wave front. Hence, for perpendicular polarization (as defined with respect to a plane wave incident on the panel) let us assume that the primary source (3.3) has only a variation in the z'x' plane, i.e. let $\phi'=0$. Substituting $\phi'=0$ in (3.3) we obtain

$$\underline{E}_h \Big|_{z=0} = E_o \hat{i}_y \cos\theta' \frac{e^{-jk_o R'}}{R'} \tag{3.3a}$$

which is similar to the field of an electric line source. For parallel polarization on the other hand, let us modify the primary source (3.3) by assuming only a

variation in the z'y' plane, i.e. $\phi' = \frac{\pi}{2}$. Substituting $\phi' = \frac{\pi}{2}$ in (3) we obtain

$$\underline{E}_h \Big|_{z=0} = (-\cos\theta' \sin\theta' \hat{i}_z + \cos^2\theta' \hat{i}_y) E_o \cos\theta' \frac{e^{-jkR'}}{R'} \qquad (3.3b)$$

$$= (\cos\theta' \hat{i}_\theta) E_o \cos\theta' \frac{e^{-ikR'}}{R'}$$

which is similar to the field of a magnetic line source. The above two results were obtained by using the expression

$$\hat{k} = \hat{r} = \sin\theta' \cos\phi' \hat{i}_x + \sin\theta' \sin\phi' \hat{i}_y + \cos\theta' \hat{i}_z$$

and where

$$R' = \sqrt{h^2 + \rho'^2}$$

$$\rho' = \sqrt{x'^2 + y'^2}$$

$$\cos\theta' = h/R'$$

Expressions (3.3) are approximations valid for the far field of a low gain small horn antenna; they show an additional cosine tapering in both the E and H plane over that of a pure dipole. As far as the $\frac{1}{r}$ variation in amplitude is concerned, this is not a good approximation in the near field; there, a faster drop-off with respect to r, such as r^{-2} or r^{-3}, would be more correct. However, since the excitation of our panel will depend largely on the pattern and phase of the horn antenna and since these are similar in the near and far field we will use (3.3) as the field of our

primary source at the panel. Hence on S_1, the $\hat{n} \times \underline{E}(\rho')$ term becomes

$$\hat{i}_z \times \underline{E}_h \Big|_{z=0} = E_o \cos\theta' \hat{i}_z \times \left[(\hat{k}' \times \hat{i}_y) \times \hat{k}' \right] \frac{e^{-jk_o R'}}{R'} \tag{3.4}$$

and the corresponding expressions using (3.3a) and (3.3b) are

$$\hat{i}_z \times \underline{E}_h \Big|_{z=0} = -E_o \hat{i}_x \cos\theta' \frac{e^{-jk_o R'}}{R'} \tag{3.4a}$$

and

$$\hat{i}_z \times E_h \Big|_{z=0} = -E_o \hat{i}_x \cos\theta'^3 \frac{e^{-jk_o R'}}{R'} \tag{3.4b}$$

Substituting the above expressions in (3.2) and performing the ∇ operation we obtain

$$\underline{E}(r) = \frac{1}{2\pi} \iint_{S_1} (\hat{i}_z \times \underline{E}_h \Big|_{z=0}) \times \frac{e^{-jk_o R}}{R} (jk_o + \frac{1}{R}) \hat{R} \, da' \tag{3.5}$$

Substituting (3.4a) we obtain

$$\underline{E}(\underline{r}) = \frac{E_o}{2\pi} \iint_{S_1} \frac{h}{R'^2} e^{-jk_o R'} \frac{e^{-jk_o R}}{R} (jk_o + \frac{1}{R}) \hat{R} \times \hat{i}_x \, da' \tag{3.5a}$$

and substituting (3.4b) we obtain

$$\underline{E}(\underline{r}) = \frac{E_o}{2\pi} \iint_{S_1} \frac{h^3 e^{-jk_o (R'+R)}}{R'^4 R} (jk_o + \frac{1}{R}) \hat{R} \times \hat{i}_x \, da' \tag{3.5b}$$

Since we are interested in the far-field transmission pattern of the panel, we can simplify the above expression by substituting the far-field approximation for R, the distance between the source and observation point. Before we do this, we should note that this might lead to a non-existing integral. For example, when we examine the above integral of (3.5a) for large values of ρ' we observe that the integrand varies as $d\rho'/\rho'^2$ which will give a convergent result upon integration. However, if the far field approximation is substituted, we see that the integrand varies as $d\rho'/\rho'$ for large ρ', giving a $\ln\rho'$ dependence for the integral, clearly a non-convergent result. One usually avoids these unpleasantries by restricting the integration to a finite surface. This approximation can usually be justified when the radiation pattern of the primary source is very sharp, such that only the central portion, primarily where the panel is located, receives appreciable excitation. If the entire S_1 plane had a source distribution whose magnitude did not vary greatly over the plane, the far field approximation would not be valid in (3.5).

We are interested in integrating over the area of the panel for obvious reasons. If we know the material composition of various panels, we can compute their transmission coefficients and substitute it in (3.5) and restricting the area of integration will allow us to make the far field approximation in (3.5) regardless of the excitation of the panel by the primary source. However, we must evaluate the contribution of the rest of the surface since it also receives excitation by the

primary source and hence acts as a Huygens secondary source and it will give us the error if we want to approximate the transmis sion field by the finite area integral. Hence, let us divide S_1 into $S_a + S_\infty$, the area of the panel plus the rest of the surface. In the integration over S_a we can make the far field approximation since R will be assumed to be always large in terms of the diffracting system dimensions, i.e.

$$R = \left| \underline{r} - \underline{\rho}' \right| \cong r - \hat{k} \cdot \underline{\rho}' + \ldots \tag{3.6}$$

Substituting this in (3.5) we obtain

$$\underline{E}(\underline{r}) = \frac{1}{j2\pi r} \underline{k}_o \times \iint_{S_a} (\hat{i}_z \times \underline{E}_h \Big|_{z=0}) e^{j\hat{k} \cdot \underline{\rho}'} da' + \iint_{S_\infty} \tag{3.7}$$

as the correct far field formulation. If we now use the electric line source approximation (3.4a) as our primary field is (3.7) we obtain

$$\underline{E}(\underline{r}) = \frac{jE_o e^{-jk_o r}}{2\pi r} \underline{k}_o x \hat{i}_x \iint_{S_a} \frac{h}{R'^2} e^{-ik_o(R' - \hat{k} \cdot \rho')} da' + \iint_{S_\infty} \quad \ldots(3.5)\ldots \tag{3.7a}$$

If we use the finite magnetic line source approximation (3.4b) we obtain

$$\underline{E}(\underline{r}) = \frac{jE_o e^{-jk_o r}}{2\pi r} \underline{k}_o x \hat{i}_x \iint_{S_a} \frac{h^3}{R'^4} e^{-jk_o(R' - \hat{k} \cdot \underline{\rho}')} da' + \iint_{S_\infty} \tag{3.7b}$$

In an effort to evaluate the integral over S_∞ we can examine various forms. For example, in polar coordinates (3.7a) can be written as

$$\underline{E}(\underline{r}) = \frac{jhE_o e^{-jk_o r}}{2\pi r} \underline{k}_o \times \hat{i}_x \iint_{S_a} \frac{e^{-jk_o(R' - \hat{k}\cdot\rho')}}{R'^2} \rho' \, d\rho' \, d\phi' -$$

$$- \frac{hE_o}{2\pi} \nabla \times \hat{i}_x \int_a^\infty \frac{e^{-jk_o R'}}{R'^2} \rho' \, d\rho' \int_0^{2\pi} \frac{e^{-jk_o\sqrt{r^2+\rho'^2-2r\rho'\sin\theta\cos(\phi'-\phi)}}}{\sqrt{r^2+\rho'^2-2r\rho'\sin\theta\cos(\phi'-\phi)}} d\phi' \tag{3.8}$$

Since $\nabla = -\nabla'$, we can also write (3.2) with the primary source (3.3a) as

$$\underline{E}(\underline{r}) = -\frac{hE_o \tilde{i}_x}{2\pi} \times \iint \frac{e^{-jk_o R'}}{R'^2} \nabla' \frac{e^{-jk_o R}}{R} da' \tag{3.9}$$

Then in rectangular coordinates

$$\underline{E}(\underline{r}) = \iint_{S_a} \ldots - \frac{-\hat{i}_x h E_o}{2\pi} \times \int_a^\infty \int_a^\infty \frac{e^{-jk_o R'}}{R'^2} \left(\frac{\partial}{\partial y'} \frac{e^{-jk_o R}}{R} \hat{i}_y + \frac{\partial}{\partial z'} \frac{e^{-jk_o R}}{R} \hat{i}_z\right) dx' \, dy'$$

$$- \int_{-a}^{-\infty} \int_{-a}^{-\infty} \ldots \tag{3.10}$$

The differentiation with respect to z' is a limit process, where a finite z' is assumed in R and then the limit as $z' \to 0$ taken after the integration is

performed. The corresponding equations for the primary source (3.3b) are identical to (3.8), (3.9), and (3.10), except that h is replaced by h^3 and R'^2 by R'^4.

Transmission Through the Panel

Let us formulate the integral over S_a in a form most suitable for calculation. A dielectric will occupy the area S_a in our later formulation. If the surface variables are expressed in spherical coordinates as

$$\begin{aligned} x' &= h \tan\theta' \cos\phi' \\ y' &= h \tan\theta' \sin\phi' \end{aligned} \tag{3.11}$$

and this substitution made in the distance R', we obtain

$$\begin{aligned} \sqrt{h^2 + x'^2 + y'^2} &= h \sec\theta' \\ \rho &= h \tan\theta' \end{aligned} \tag{3.12}$$

Similarly the $\hat{k} \cdot \underline{\rho}'$ term in (3.7) or (3.8) can be written as

$$\hat{k} \cdot \underline{\rho}' = \sin\theta(x' \cos\phi + y' \sin\phi) = h \sin\theta \tan\theta' \cos(\phi' - \phi) \tag{3.13}$$

The electric field of (3.7a) or (3.8) can then be expressed as

$$\underline{E}(\underline{r}) = \frac{jE_o e^{-jk_o r}}{2\pi r} \underline{k}_o x \hat{i}_x \iint_{S_a} \frac{e^{-jk_o h \left[\sec\theta' - \sin\theta \tan\theta' \cos(\phi' - \phi)\right]}}{h \sec^2\theta'} da' + \iint_{S_\infty} \tag{3.14}$$

Combining this with the expression for surface area element

$$\rho' d\rho' \, d\phi' = h^2 \tan\theta' \sec^2\theta' \, d\theta' d\phi'$$

we obtain for the integral over the area S_a

$$\underline{E}(\underline{r}) \cong \frac{jE_o e^{-ik_o r}}{2\pi r} \underline{k}_o x \hat{i}_x \iint_{S_a} e^{-jk_o h \left[\sec\theta' - \sin\theta \tan\theta' \cos(\phi' - \phi)\right]} h \tan\theta' d\theta' d\phi' \, . \tag{3.15}$$

The corresponding result for (3.7b) can be obtained from (3.14) or (3.15) by dividing the integrand of (3.14) or (3.15) by $\sin^2\theta'$

a) One-dimensional approximation

In order to make the integrations more tractable, let us confine ourselves to the transmission patterns in the E-plane (zy plane or $\phi = \pi/2$ plane) and the H-plane (zx plane or $\phi = 0$ plane). Furthermore, when considering the H-plane (E-plane) pattern, let us also assume that the entire structure is infinite in the y-dimension (x dimension), i.e. let us make a one-dimensional approximation. Instead of a spherical source, we should now consider a line source. However, we pointed out before that we are primarily interested in changes of phase across the panel and that variations in amplitude should be of secondary importance. Since the phase dependence of a Hankel function is the same as that of a point source, we need not make any changes in the primary source.

The H-plane pattern of a one-dimensional source can be obtained from (3.14) by substituting $(\phi'-\phi)=0$, $\hat{k}\times\hat{i}_x=\hat{i}_y\cos\theta$, $x'=h\tan\theta'$, $dx'=h\sec^2\theta'd\theta'$. We obtain

$$\underline{E}(r,\theta,0)=\frac{jE_o e^{-jk_o r}}{2\pi r}\hat{i}_y\cos\theta\int_{-\theta_a}^{\theta_a} e^{-jk_o h\left[\sec\theta'-\sin\theta\tan\theta'\right]}d\theta'+\int_{S_\infty} \tag{3.16a}$$

The E-plane pattern can be obtained similarly from (3.7b) and (3.11) - (3.13), with the substitutions $(\phi'-\phi)=0$, $\hat{k}\times\hat{i}_x=\hat{i}_\theta$, $y'=h\tan\theta'$, $dy'=h\sec^2\theta'd\theta'$ as

$$\underline{E}(r,\theta,\frac{\pi}{2})=\frac{jE_o e^{-ik_o r}}{2\pi r}i_\theta\int_{-\theta_a}^{\theta_a}\cos^2\theta' e^{-jk_o h\left[\sec\theta'-\sin\theta\tan\theta'\right]}d\theta' \tag{3.16b}$$

The integral over S_∞ (of (3.16a) can be written from (3.8) as

$$\frac{1}{2}\int_{S_\infty}=-\frac{hE_o}{2\pi}\nabla\times\hat{i}_x\int_a^\infty\frac{e^{-jk_o\sqrt{h^2+x'^2}}}{h^2+x'^2}\frac{e^{-jk_o\sqrt{r^2+x'^2-2rx'\sin\theta}}}{\sqrt{r^2+x'^2-2rx'\sin\theta}}dx' \tag{3.17a}$$

or from (3.10) as

$$\frac{1}{2}\int_{S_\infty}=\frac{hE_o}{2\pi}\hat{i}_x\times\frac{\partial}{\partial z}\int_a^\infty\frac{e^{-jk_o\sqrt{h^2+x'^2}}}{h^2+x'^2}\frac{e^{-jk_o\sqrt{(x-x')^2+z^2}}}{\sqrt{(x-x')^2+z^2}}dx' \tag{3.18a}$$

The corresponding integrals over S_∞ for (3.16b) can be written as

$$\frac{1}{2}\int_{S_\infty} = \frac{-h^3 E_o}{2\pi}\nabla x\hat{i}_x\int_a^\infty \frac{e^{-jk_o\sqrt{h^2+y'^2}}}{(h^2+y'^2)^2}\,\frac{e^{-ik_o\sqrt{r^2+y'^2-2ry'\sin\theta}}}{\sqrt{r^2+x'^2-2rx'\sin\theta}}dy' \tag{3.17b}$$

and as

$$\frac{1}{2}\int_{S_\infty} = \frac{h^3 E_o}{2\pi}\hat{i}_x x\frac{\partial}{\partial z}\int_a^\infty \frac{e^{-jk_o\sqrt{h^2+y'^2}}}{(h^2+y'^2)^2}\,\frac{e^{-jk_o\sqrt{(y-y')^2+z^2}}}{\sqrt{(y-y')^2+z^2}}dy' \tag{3.18b}$$

or as

$$\frac{1}{2}\int_{S_\infty} = \hat{i}_\theta\frac{h^3 E_o}{2\pi}\int_a^\infty \frac{e^{-jk_o(R'+R)}}{R'^4 R}(jk_o+\frac{1}{R})dy'$$

b) Transmission from a dielectric medium into free space

If in Fig. 3.2 the half space $z<0$ is occupied by a dielectric medium with ϵ_r and μ_r the relative permittivity and permeability, the transmission coefficient for an incident wave traveling from the dielectric (incident at angle θ') into free space (emerging at angle θ) is

$$T_\perp = \frac{\sqrt{\sin 2\theta' \sin 2\theta}}{\sin(\theta'+\theta)} \tag{3.19}$$

for $\underline{E}^i$ normal to the plane of incidence and

$$T_{//} = \frac{\sqrt{\sin 2\theta' \sin 2\theta}}{\sin(\theta'+\theta)\cos(\theta'-\theta)} \qquad (3.20)$$

with $\underline{E}^i$ parrellel to the plane of incidence. If the primary source is again a small horn antennas with radiation properties as given by (3.3) the electric field in the one-dimensional formulation can be expressed from (3.16) as

$$E \sim \int T(\theta') e^{-jh(k_d \sec\theta' - k_o \sin\theta \tan\theta')} d\theta' + \int_{S_\infty} T(\theta') \ldots \qquad (3.21)$$

The integral over S_∞ is the same as given by (3.17) or (3.18) except that the integrand is multiplied by the transmission coefficient T. Substituting T, the H-plane (zx plane) transmission field pattern can be determined from

$$\underline{E}_\perp (r,\theta,0) = \frac{jE_o e^{-jk_o r}}{2\pi r} \hat{i}_y \cos\theta \int_{-\theta_a}^{\theta_a} \left[1 - \frac{\sin(\theta'-\theta)}{\sin(\theta'+\theta)}\right]$$

$$\cdot\, e^{-jk_o h(\sqrt{\mu_r \epsilon_r} \sec\theta' - \sin\theta \tan\theta')} d\theta' + \int_{S_\infty} T_\perp(\theta') \ldots \qquad (3.22)$$

and the E-plane (zy plane) transmitted field is

$$\underline{E}_{//} (r,\theta,\tfrac{\pi}{2}) = \frac{jE_o e^{-jk_o r}}{2\pi r} \hat{i}_\theta \int_{-\theta_a}^{\theta_a} \frac{\sin(\theta'+\theta) - \sin(\theta'-\theta)}{\sin(\theta'+\theta)\cos(\theta'-\theta)} \cos^2\theta'$$

$$e^{-jk_o h(\sqrt{\mu_r \epsilon_r} \sec\theta' - \sin\theta \tan\theta')} d\theta' + \int_{S_\infty} T_{//}(\theta') \ldots \qquad (3.23)$$

c) Transmission through a non-magnetic, dielectric panel

We will continue our physical optics type of analysis by considering radiation from a dielectric panel with $\mu=\mu_o$ which is excited from the other side by the primary source (3.3). The length of the panel is 2a, thickness is d. The panel geometry is shown in Fig. 3.3.

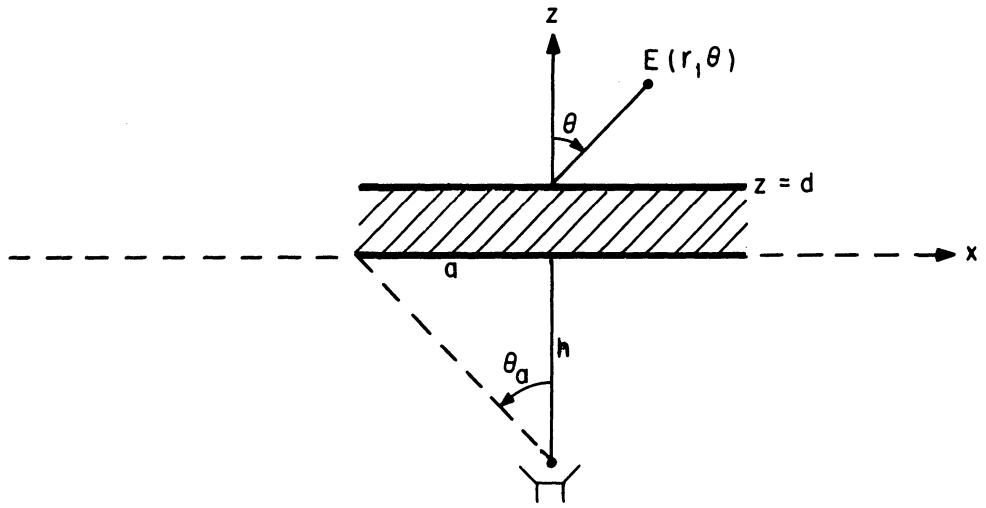

DIELECTRIC PANEL EXCITED BY A PRIMARY SOURCE

The transmission coefficient for such a panel when a plane wave is incident from the region $z<0$ at an angle θ' is given by

$$T = \frac{(1-r^2)e^{jd(k_o\cos\theta' - k_z')}}{1-r^2e^{-j2k_z'd}} \qquad (3.24)$$

where $k'_z = k_o\sqrt{\epsilon_r - \sin^2\theta'}$ and the reflection coefficient at a dielectric interface for parallel polarization with respect to the plane of incidence is

$$r = r_{//} = \frac{\epsilon_r \cos\theta' - \sqrt{\epsilon_r - \sin^2\theta'}}{\epsilon_r \cos\theta' + \sqrt{\epsilon_r - \sin^2\theta'}} \tag{3.25}$$

and for perpendicular polarization

$$r_\perp = \frac{\cos\theta' - \sqrt{\epsilon_r - \sin^2\theta'}}{\cos\theta' + \sqrt{\epsilon_r - \sin^2\theta'}} \tag{3.26}$$

Substituting these in (3.16) the H-plane transmitted field becomes

$$\underline{E}_\perp(r,\theta,0) = \frac{jE_o e^{-jk_o r}}{2\pi r}\hat{i}_y \cos\theta \int_{-\theta_a}^{\theta_a} T(r_\perp, d, \theta') e^{-jk_o h(\sec\theta' - \sin\theta\tan\theta')} d\theta' + \int_{S_\infty} \tag{3.27}$$

and the E-plane transmitted field is

$$\underline{E}_{//}(r,\theta,\tfrac{\pi}{2}) = \frac{jE_o e^{-jk_o r}}{2\pi r}\hat{i}_\theta \int_{-\theta_a}^{\theta_a} T(r_{//}, d, \theta') e^{-jk_o h(\sec\theta' - \sin\theta\tan\theta')} \cos^2\theta' d\theta' + \int_{S_\infty} \tag{3.28}$$

the integrals over S_∞ are again given by (3.17) or (3.18).

d) Transmission through an anisotropic dielectric panel

The next case that we would like to consider is an anisotropic dielectric panel with tensor permittivity $\bar{\bar{\epsilon}}$ and permeability $\bar{\bar{\mu}}$. The panel geometry is the same as that in Fig. 3.3. It is assumed that the material can be electrically

polarized in the z and y directions and magnetically in the x direction, such that

$$\bar{\bar{\epsilon}} = \begin{bmatrix} \epsilon & 0 & 0 \\ 0 & \epsilon_1 & 0 \\ 0 & 0 & \epsilon_1 \end{bmatrix} \qquad \bar{\bar{\mu}} = \begin{bmatrix} \mu_1 & 0 & 0 \\ 0 & \mu_o & 0 \\ 0 & 0 & \mu_o \end{bmatrix} \tag{3.29}$$

The transmission coefficient can then be determined as

$$T = \frac{(1-r^2)e^{j(k_z - k'_z)d}}{1-r^2 e^{-j2k'_z d}} \tag{3.30}$$

where

$$k_z = k_o \cos\theta'$$

$$k'_z = k_o \sqrt{K_m (K'_e - \sin^2\theta')} \tag{3.31}$$

$$K'_e = (\epsilon/\epsilon_o)K_e, \quad K_e = \epsilon_1/\epsilon_o, \quad K_m = \mu_1/\mu_o$$

The interface reflection coefficient r for the perpendicular polarization is

$$r = \frac{\sqrt{K_m}\cos\theta' - \sqrt{K'_e - \sin^2\theta'}}{\sqrt{K_m}\cos\theta' + \sqrt{K'_e - \sin^2\theta'}} \tag{3.32}$$

Hence, the H-plane (xz plane) transmitted field is given from (3.16) as

$$\underline{E}_{\perp}(r,\theta,0)=\frac{jE_o e^{-jk_o r}}{2\pi r}\hat{i}_y \cos\theta \int_{-\theta_a}^{\theta_a} T(r_{\perp},d,\theta')e^{-jk_o h(\sec\theta'-\sin\theta\tan\theta')}d\theta' + \int_{S_\infty} \tag{3.33}$$

The S_∞ integration is given by (3.17a) or (3.18a).

For the other polarization, with E vector parallel to the plane of incidence the transmission coefficient is that of (3.30). The interface reflection coefficient is given by

$$r_{//}=\frac{K'_e\cos\theta' - \sqrt{K_m K'_e - \sin^2\theta'}}{K'_e\cos\theta' + \sqrt{K_m K'_e - \sin^2\theta'}} \tag{3.34}$$

and k'_z should be replaced by β'_z where

$$\beta'_z = k_o\sqrt{K_m K'_e - \sin^2\theta'} \tag{3.35}$$

Hence for this polarization the transmission coefficient is

$$T_{//}=\frac{(1-r_{//}^2)e^{j(k_z-\beta'_z)d}}{1-r_{//}^2 e^{-j2\beta'_z d}} \tag{3.36}$$

The transmitted electric field in the E-plane (zy plane) is then from (3.16b)

$$\underline{E}_{//}(r,\theta,\tfrac{\pi}{2})=\frac{jE_o e^{-jk_o r}}{2\pi r}\hat{i}_\theta \int_{-\theta_a}^{\theta_a} T_{//}(r_{//},\phi,\theta')\cos^2\theta' e^{-jk_o h\left[\sec\theta'-\sin\theta\tan\theta'\right]}d\theta' + \int_{S_\infty} \tag{3.37}$$

The integral over S_∞ is given by (3.17b) or (3.18b).

e) Transmission through an anisotropic dielectric panel excited by a Magnetic dipole source

If a small slot antenna, with dimensions much smaller than a wavelength is used as a primary radiator, a good approximation to its radiation pattern is the field of a magnetic dipole oriented such that its axis is parallel to the long dimension of the slot. Hence, let us use the far field of a magnetic dipole, oriented parellel to the x-axis as primary source.

$$\underline{E}'(r,\theta,\phi) = E_o(\hat{k}' \times \hat{i}_x)\frac{e^{-jkR'}}{R'} \tag{3.38}$$

To use the plane wave transmission coefficient we will again make use of the one-dimensional approximation. This we hope will give good results if we confine our interest to the H-plane and E-plane transmission patterns of the dielectric panel. As before, we will use the H-plane (zx plane) pattern of the primary source as the excitation field for the dielectric panel when we desire the H-plane (zx) transmitted far field of the panel. The H-plane excitation pattern of a magnetic dipole can be obtained from (3.38) by substituting $\phi'=0$. Thus,

$$\underline{E}'(r', \theta', 0) = E_o \cos\theta' \hat{i}_y \frac{e^{-ikR'}}{R'} \tag{3.39}$$

and the corresponding $n \times E'$ to be used in the integrand of (3.16a) is

$$\hat{i}_z \times \underline{E}'\Big|_{z=0} = -E_o \cos\theta' \hat{i}_x \frac{e^{-jkR'}}{R'} \tag{3.40}$$

Hence, the transmitted far field of the anisotropic dielectric panel, using $T_\perp$ (or (3.30)) is

$$\underline{E}_\perp(r,\theta,0) = \frac{jE_o e^{-jk_o r}}{2\pi r} \hat{i}_y \cos\theta \int_{-\theta_a}^{\theta_a} T_\perp e^{-jk_o h(\sec\theta' - \sin\theta \tan\theta')} d\theta' + \int_{S_\infty} \tag{3.41}$$

which is identical to (3.37).

The E-plane (zy plane) transmitted far field pattern from the panel can be obtained similarly by using the E' plane pattern of the primary source. Hence the E' plane pattern of the magnetic dipole can be obtained from (3.38) by substituting $\phi' = \frac{\pi}{2}$,

$$\begin{aligned} \underline{E}'(r',\theta',\tfrac{\pi}{2}) &= E_o(\cos\theta' \hat{i}_y - \sin\theta' \hat{i}_z)\frac{e^{-jkR'}}{R'} \\ &= E_o \hat{i}_\theta \frac{e^{-jkR'}}{R'} \end{aligned} \tag{3.42}$$

The $\hat{n} \times E'$ term becomes

$$\hat{i}_z \times \underline{E}'\Big|_{z=0} = -E_o \cos\theta' \hat{i}_x \frac{e^{-jkR'}}{R'} \tag{3.43}$$

The transmitted field in the E-plane is then

$$\underline{E}_{//}(r,\theta,\frac{\pi}{2}) = \frac{jE_o e^{-jk_o r}}{2\pi r}\hat{i}_\theta \int_{-\theta_a}^{\theta_a} T_{//} e^{-jk_o h(\sec\theta'-\sin\theta\tan\theta')} d\theta' + \int_{S_\infty} \tag{3.44}$$

f) Transmission through an anisotropic dielectric panel excited by a Ferrite Slot Antenna

In Fig. 1.1 of the Introduction the radiation patterns of a ferrite antenna are shown. When the experimental radiation patterns from a ferrite loaded slot antenna are examined it is seen that neither an electric nor a magnetic dipole source approximates these patterns well, at least not in both H and E planes. The agreement between the theoretical and experimental patterns is better for the H-plane patterns but no agreement exists for the E-plane patterns. In view of this disagreement let us choose a simple function which shows the characteristic behavior of the E and H plane patterns for a ferrite slot antenna with a flange (3 ft. x 3 ft. ground plane). From an examination of the experimental patterns, we see that in the H-plane the pattern is predicted well by

$$\underline{E}'_y = \hat{i}_y \cos\theta' \tag{3.45}$$

This approximation can also be obtained by substituting $k_o a \ll 1$ in the E_ϕ expression of (1.2) in the Introduction. The E-plane pattern can be approximated by

$$\underline{E}'_\theta = \hat{i}_\theta \cos\theta' \tag{3.46}$$

It should be noted that (3.46) cannot be obtained by substituting $k_o b \ll 1$ in (1.1) of the Introduction. Hence this approximaton is not as good as (3.45).

The transmitted H-plane far field from the anisotropic dielectric panel, using (3.45) is then identical to the expressions given by (3.33) or (3.41).

The transmitted E-plane far field from the anisotropic dielectric panel, using (3.46) is then given by

$$\underline{E}_{//}(r,\theta,\frac{\pi}{2}) = \frac{jE_o e^{-jk_o r}}{2\pi r} \hat{i}_\theta \int_{-\theta_a}^{\theta_a} T_{//} \cos\theta' e^{-jk_o h(\sec\theta' - \sin\theta \tan\theta')} d\theta' + \int_{S_\infty} \tag{3.47}$$

Conclusion

At present, the integrals for the transmitted electric field, both for the E-plane and H-plane are being computed. These will be compared to the experimental data, and since this data will be presented as power patterns, the final computations are for $|E|^2$. The error integrals, i.e. the integrals over S_∞ will be determined approximately, either by using the first term in a power series expansion or by applying a stationary phase technique. Since the panel dimension is a, and since the evaluated integrals over S_∞ will behave as $1/a$ raised to some power, the S_∞ integrals will give us the error committed when the transmitted field is obtained from the integration over the area of the panel (instead of all space) only.

A preliminary analysis of the computed data for the integral (3.41) which represents the transmitted electric field in the H-plane can be given in the following table. It is a tabulation of the half power beamwidth for five dielectric panels

h		1"	2"	160"
$\mu = 1$	$\epsilon = 2$	88^o	82^o	64^o
$\mu = 1$	$\epsilon = 4$	87^o	84^o	68^o
$K_m = .755$	$K_e = 1.65$	86^o	84^o	64^o
$K_m = .755$	$K_e = 3.3$	90^o	84^o	68^o
$K_m = .755$	$K_e = 6.6$	88^o	87^o	64^o

Table 3-1: Tabulation of Half Power Beamwidth in the H-plane for Five Dielectric Panel for a Frequency of 370 Mc

The distance of the primary source to the panel is given by h. The last column for h=160", is when the primary source is in the far field; hence it should be comparable to a plane wave source. Plane wave solutions for ordinary dielectric panels are known and can be compared to our case. Richmond (1965) calculated the transmitted field for a 2.50λ dielectric slab of $\mu = 1$, $\epsilon = 4$, by a physical optics method and by an exact integration method. His results and our calculations agree excellently at the corresponding frequency. It should be pointed out that the rows in the above table correspond to an ordinary dielectric panel of $\epsilon=2$ and $\epsilon = 4$ in the first and second row respectively. The third row corresponds to an

anisotropic artificial dielectric which consist of discs in free space, the fourth row corresponds to discs in a dielectric of $\epsilon=2$, and the fifth row to discs in a dielectric of $\epsilon=4$. If we plot beamwidth angle θ_o versus distance h using the three points given in the table, it is suggested that we obtain a graph as follows:

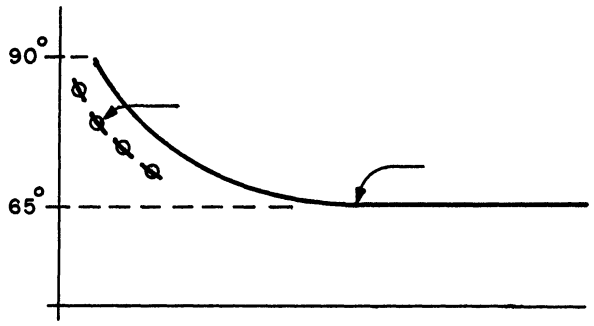

FIG. 3.4: BEAMWIDTH θ_o VERSUS DISTANCE h OF A PRIMARY SOURCE FROM A DIELECTRIC PANEL

It is seen that optimum directivity is obtained when the illumination of the panel has a uniform phase along the panel which corresponds to a plane wave incident normally on the panel. Apparently, the different dielectric properties of the panels do not have significant effects upon the directivity. The spacing h of the primary souce determines the phase along the panel. Hence, for small values of h, when the phase is non-uniform, the directivity is poorer than for a more uniform phase front. The experimental data for h between 3/4" to 2" agrees

with the calculated data except that the beamwidth is sharper by about 7^{o} for all values of h. This constant difference could be due to the error in the one-dimensional approximation and the failure to include the integral over all space outside the dielectric panel surface, i.e., the integral over S_{∞}. However, the important characteristic, namely the behavior of the beamwidth versus primary source spacing h agree when the calculated data is compared to the experimental data.

IV
EXPERIMENTAL MEASUREMENTS

The experimental phase of the research is concentrated at present on two aspects. The first concerns itself with VSWR measurements of the Radant structure whereas the second part has for its main objective the determination of the half power beam width θ_o in the E and H planes.

The VSWR measurements are completed. The results can best be summarized in Fig. 4.1 and 4.2. For these measurements the radant loops were oriented parallel to the E field. In this position the frequency at which minimum VSWR occured, changed from 300 Mc to 346 Mc as a function of the spacing between the array panel and the ferrite slot. With the loops normal to the E field no change in the VSWR was observed. At the higher frequencies (450-780 Mc) with the radant loops either parallel or normal to the E field, no change in the VSWR was observed. The VSWR was always less than 2:1 and it appeared that most of the power was absorbed by the ferrite material at the higher frequencies.

The above measurements were performed with the ferrite loaded slot mounted flush in an 18 inch[+] square ground plane. The radant structure was mounted so that the spacing between it and the ground plane could be changed in increments from 3/8" to 2".

[+] All of the patterns were made with a 48" square ground plane.

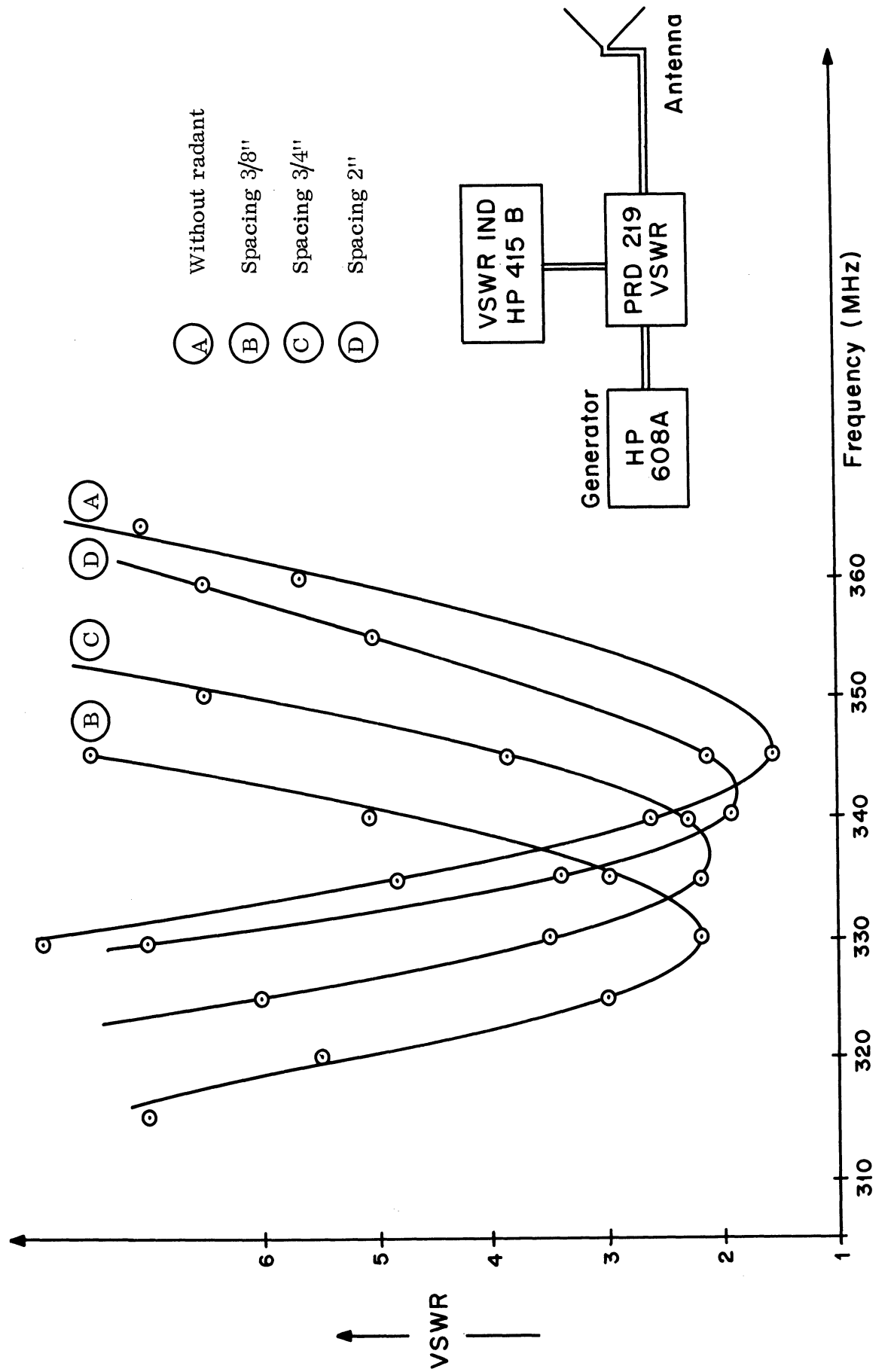

FIG. 4.1: STANDING WAVE RATIO VS FREQUENCY: PRIMARY SOURCE FERRITE-LOADED ANTENNA (Loops in Parallel with E Field)

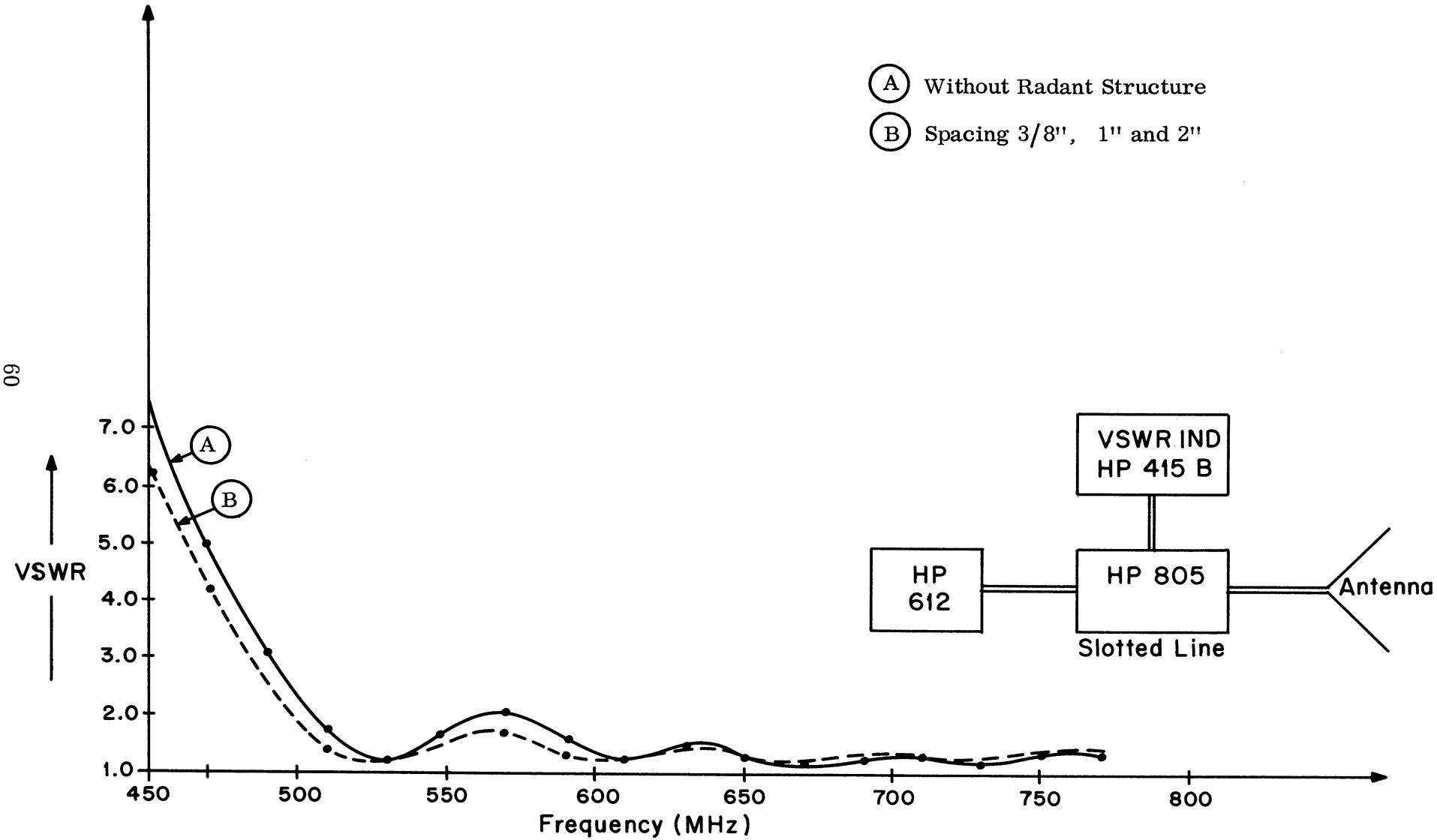

FIG. 4.2: STANDING WAVE RATIO VS FREQUENCY: PRIMARY SOURCE FERRITE LOADED ANTENNA
(Loops in Parallel with the E Field)

To perform the pattern measurements the radant structure was used as a receiver. A corner reflector antenna was used as a transmitter. Table 4.1 lists the beamwidth variation as a function of spacing between the primary source and the array panel. This variation is also shown in Fig. 4.3.

We can make the following general observation

(i) The H-plane is more directive than the E-plane

(ii) The directivity improvement versus radant spacing is higher in E-plane ($\approx 20\%$) then in the H-plane ($\approx 10\%$)

(iii) In both planes the directivity improves with a larger radant spacing

(iv) For a 3/8" spacing no remarkable change in pattern shape was observed (375 Mc)

(v) For a 2" spacing the E and H plane patterns are given in Fig. 4.6 and 4.7 (375 Mc)

(vi) The E and H plane pattern of the primary source above are given in Fig. 4.4 and 4.5 (375 Mc)

Frequency (Mc)		Spacing				
		No Radant	3/8"	1"	$1\frac{1}{2}$"	2"
331	$\vec{E}$	134^o	134^o	126^o	116^o	110^o
	$\vec{H}$	—	—	—	—	—
335	$\vec{E}$	136^o	130^o	125^o	114^o	108^o
	$\vec{H}$	116^o	116^o	110^o	—	100^o
341	$\vec{E}$	138^o	132^o	125^o	110^o	104^o
	$\vec{H}$	—	—	—	—	—
348	$\vec{E}$	140^o	140^o	122^o	115^o	108^o
	$\vec{H}$	110^o	110^o	102^o	—	100^o
375	$\vec{E}$	135^o	130^o	124^o	108^o	102^o
	$\vec{H}$	82^o	78^o	72^o	—	72^o

Table 4-1: Half-power Beam Width Expressed in Degrees as Function of Spacing, h, and Frequency

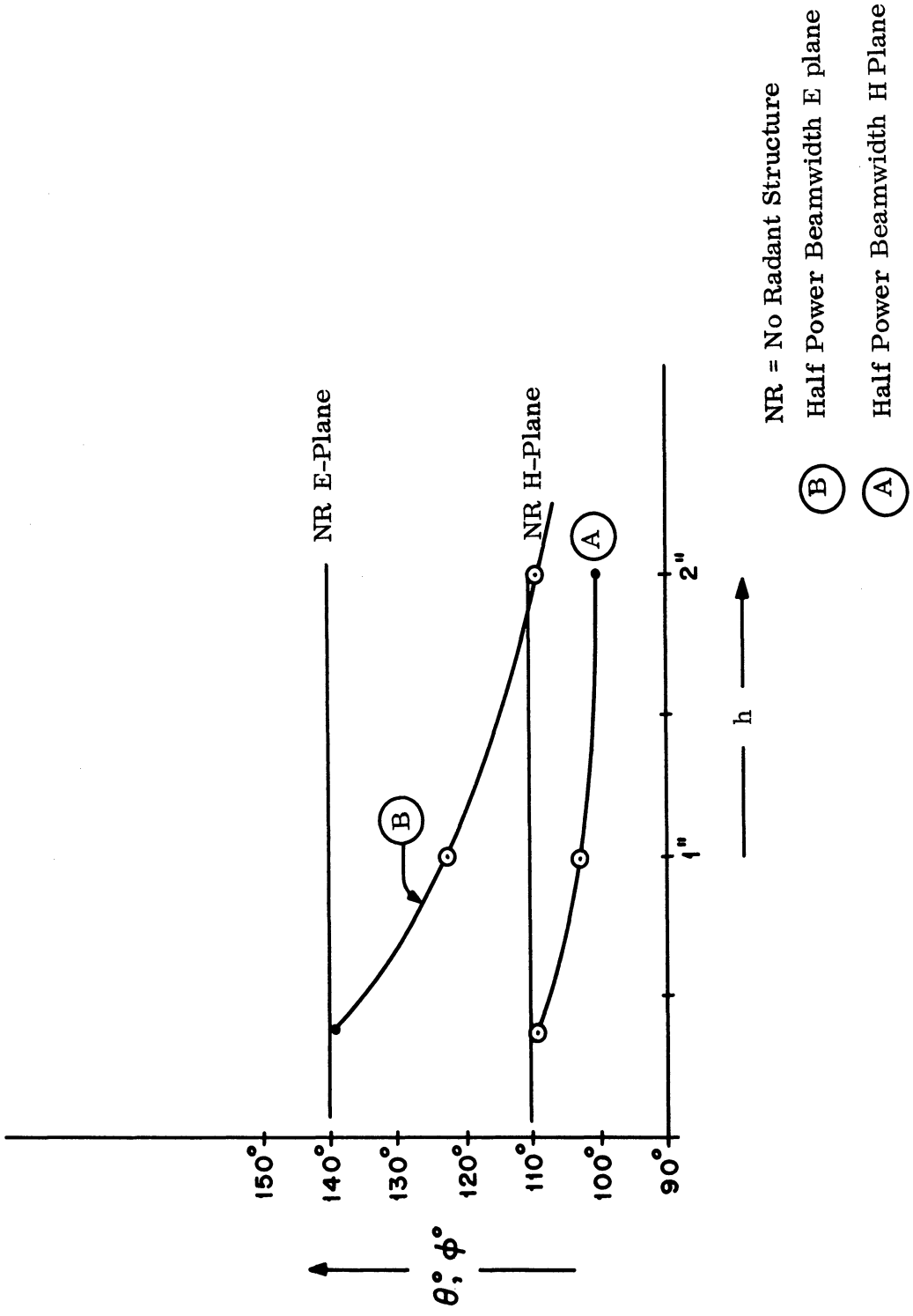

FIG. 4.3: HALF POWER BEAM AS FUNCTION OF SPACING (348 Mc)

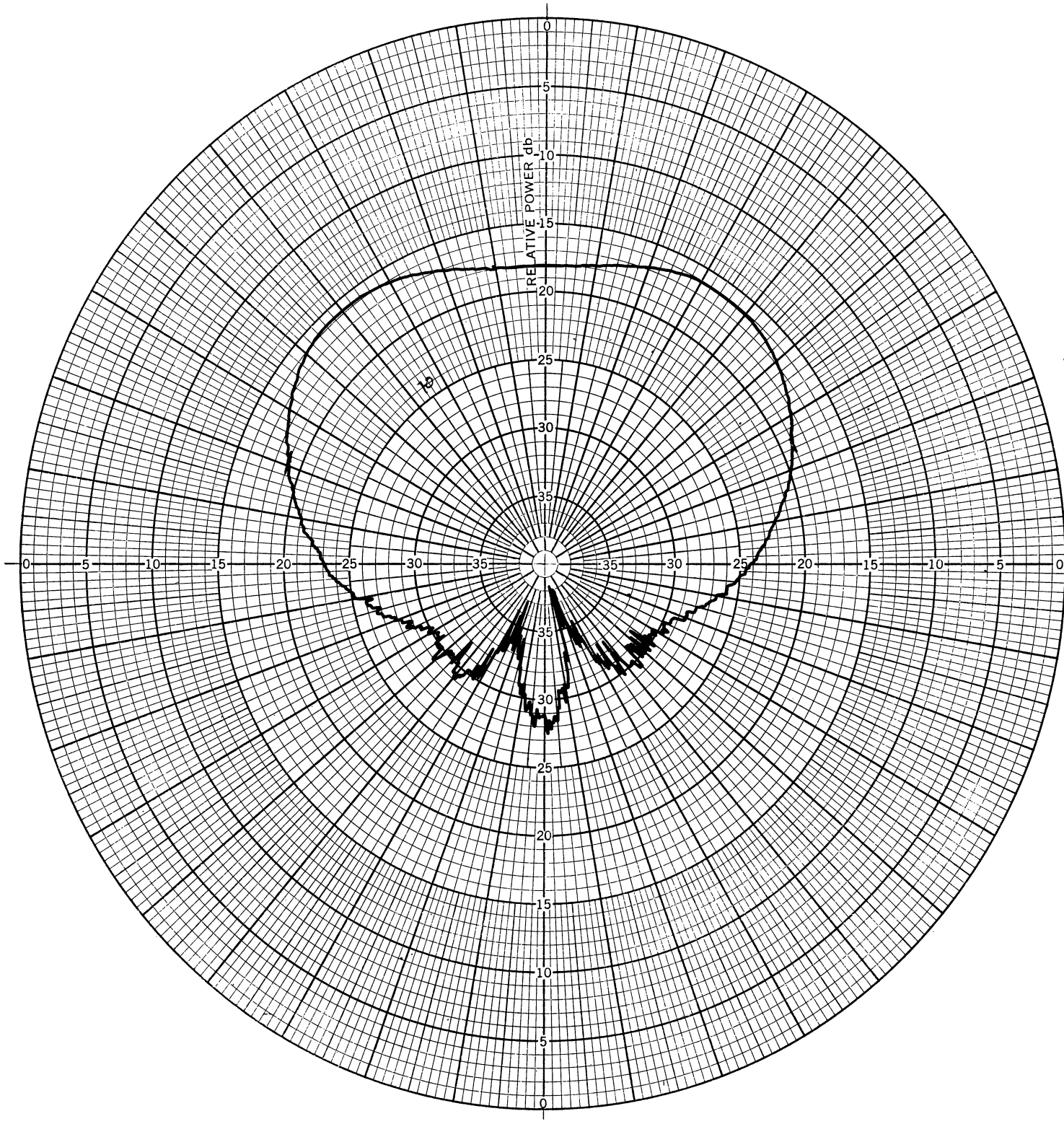

FIG. 4.4: E-PLANE PATTERN OF THE FERRITE SLOT ANTENNA WITH A 48" GROUND PLANE

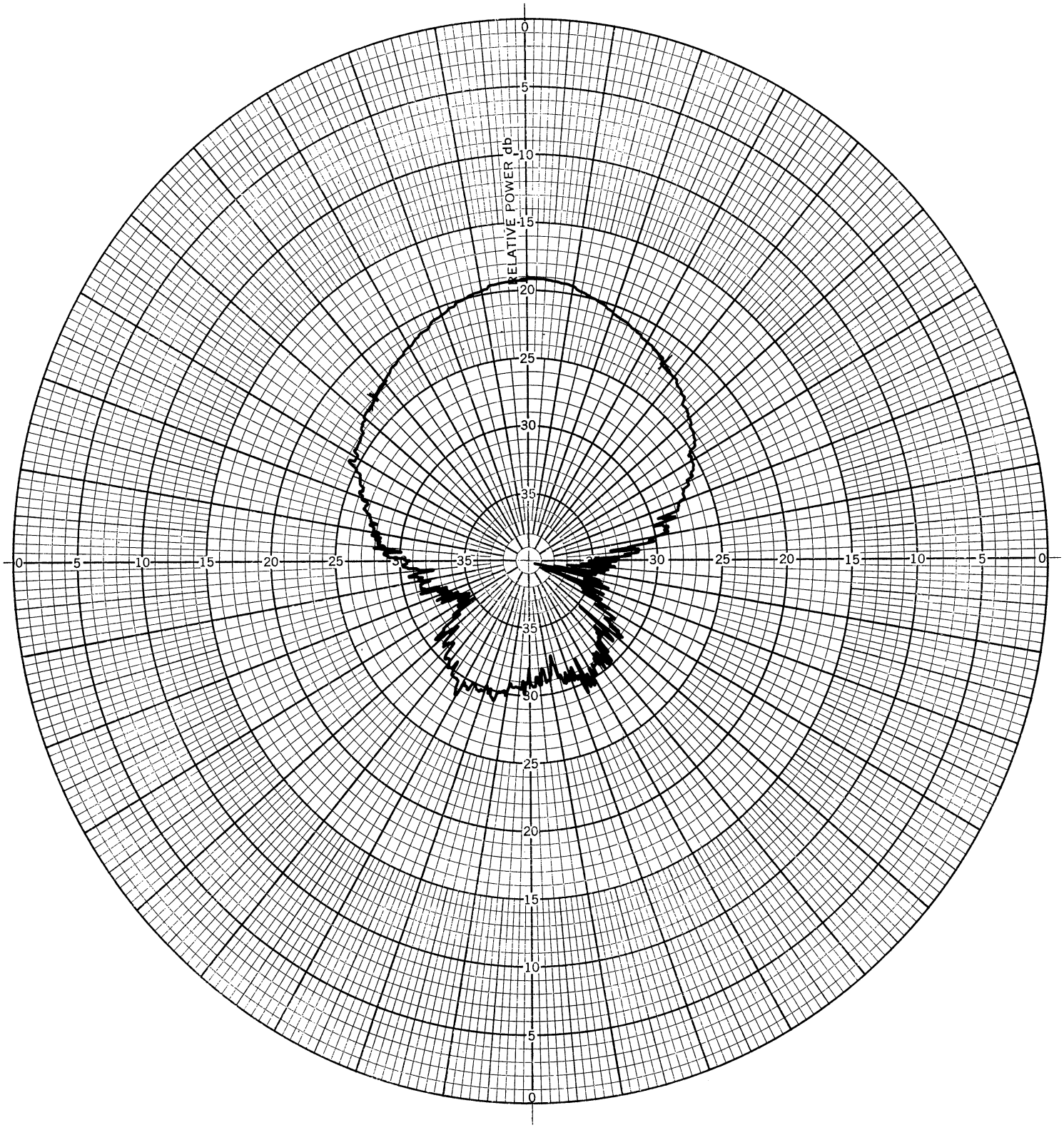

FIG. 4.5: H-PLANE PATTERN OF THE FERRITE SLOT ANTENNA WITH A 48" GROUND PLANE

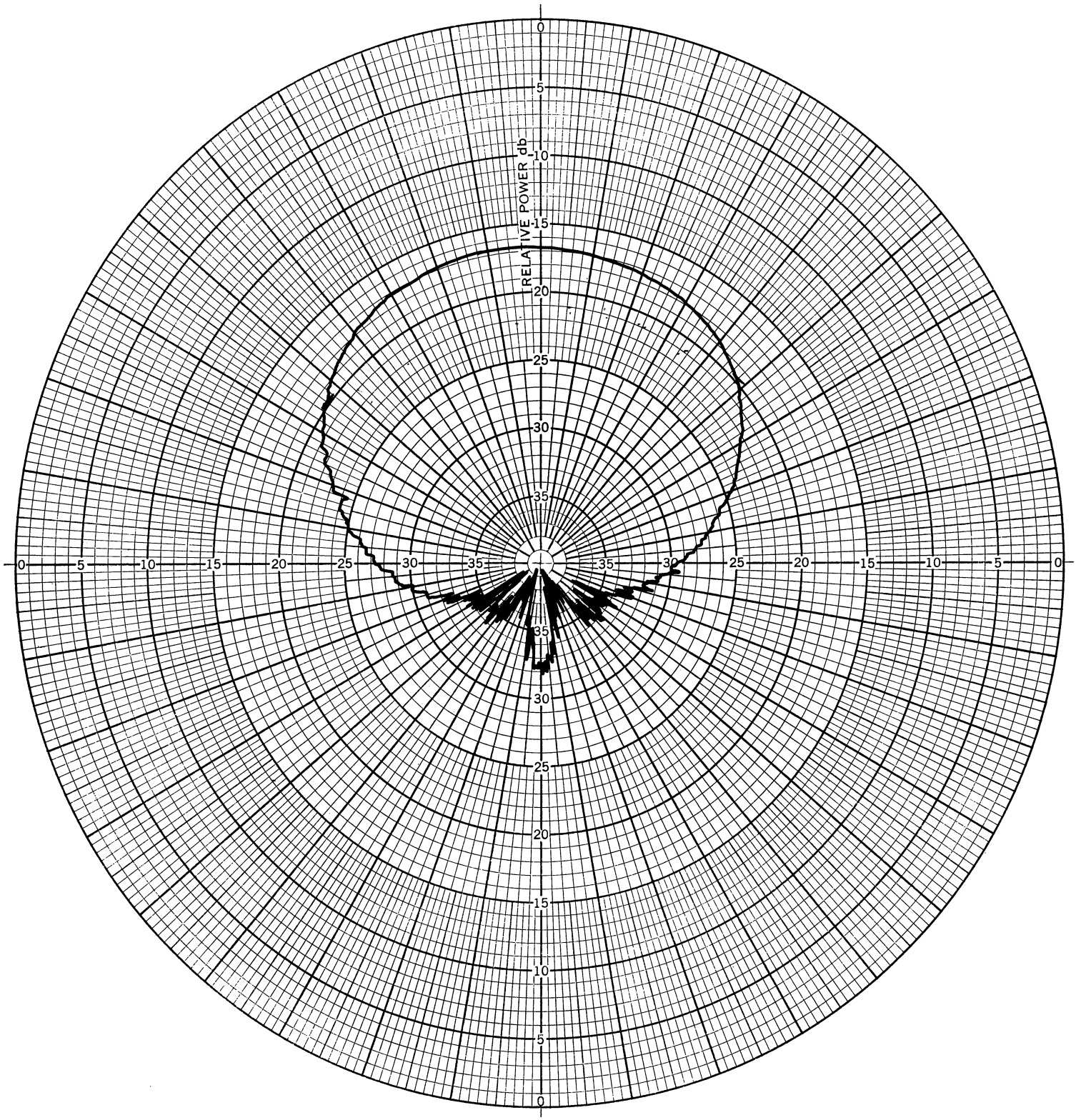

FIG. 4.6: E-PLANE PATTERN OF THE RADANT (h, the slot antenna to array panel spacing is 2")

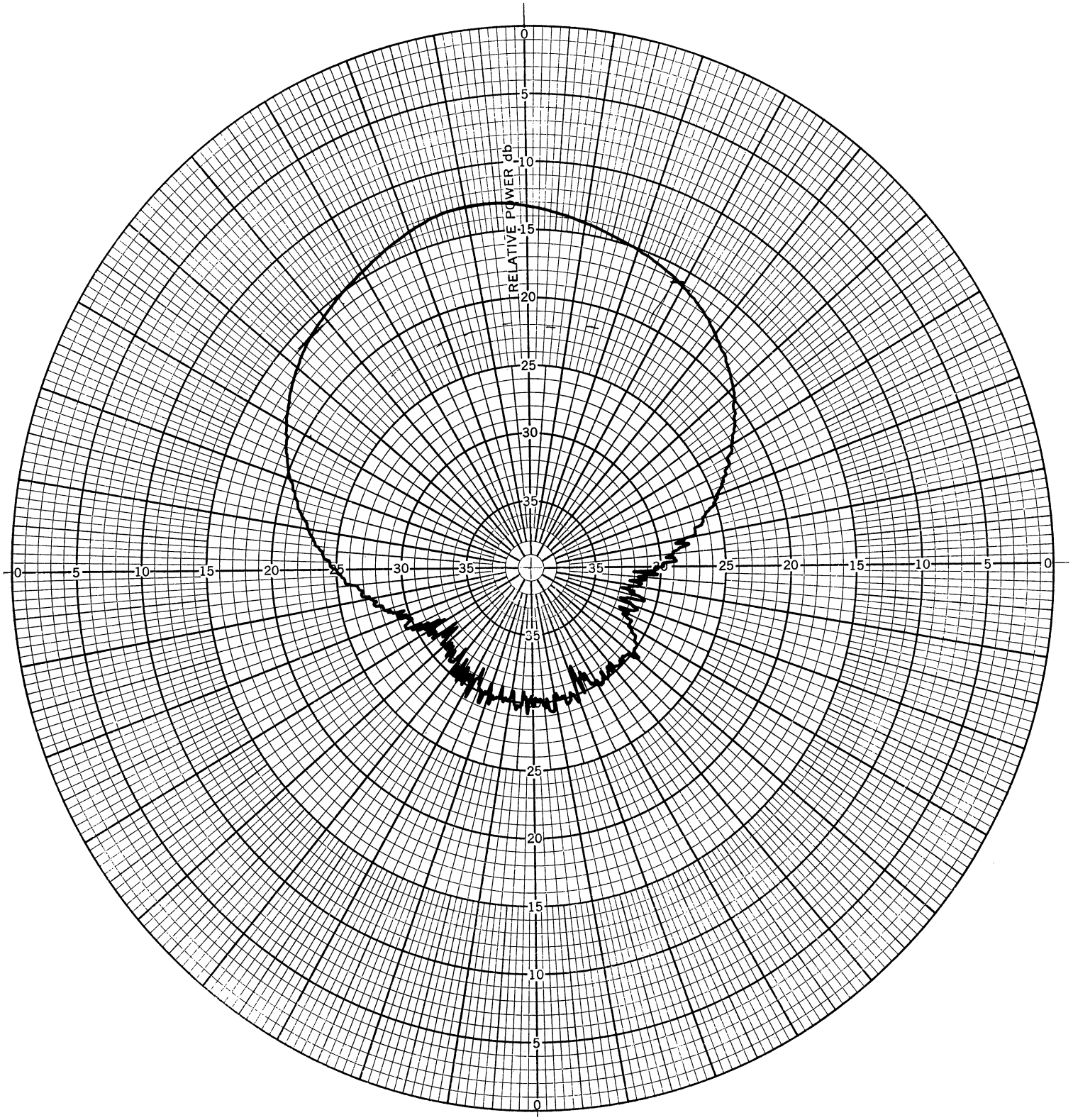

FIG. 4.7: H-PLANE PATTERN OF THE RADANT (h=2")

REFERENCES

Adams, A.T. (1964), "The Rectangular Cavity Slot Antenna with Homogeneous Isotropic Loading," University of Michigan Cooley Electronics Laboratory, Technical Report 147, AD 603657.

Collin, R.E. (1960), Field Theory of Guided Waves, McGraw-Hill Book Company, New York, Chapter 12.

Collin, R.E. (1960), Field Theory of Guided Waves, McGraw-Hill Book Company, New York, pp 520-525.

Jackson, J.D. (1962), "Classical Electrodynamics," John Wiley, New York, p.287.

Stratton, J.A. (1941), Electromagnetic Theory, McGraw-Hill Book Company, New York, p.512.

Tai, C.T. (1952), "Quasi-Static Solution for Diffraction of a Plane Electromagnetic Wave by a Small Oblate Spheroid," Trans. PGAP, Vol.1, pp 13-36.

Richmond, J.H.(1965), "Scattering by a Dielectric Cylinder of Arbitrary Cross Section Shape," Trans. PTGAP, Vol. AP-13, pp 334-341.

Unclassified

Security Classification

DOCUMENT CONTROL DATA - R&D

(Security classification of title, body of abstract and indexing annotation must be entered when the overall report is classified)

1. ORIGINATING ACTIVITY (Corporate author)	2a. REPORT SECURITY CLASSIFICATION
The University of Michigan Radiation Laboratory Department of Electrical Engineering Ann Arbor, Michigan	Unclassified
	2b. GROUP

3. REPORT TITLE

Radant Analysis Studies

4. DESCRIPTIVE NOTES *(Type of report and inclusive dates)*

Interim Report No. 1

5. AUTHOR(S) *(Last name, first name, initial)*

Tai, C-T and Plonus, M.A. and Andrade, E.S.

6. REPORT DATE	7a. TOTAL NO. OF PAGES	7b. NO. OF REFS
August 1965	68	6

8a. CONTRACT OR GRANT NO.	9a. ORIGINATOR'S REPORT NUMBER(S)
AF 33(615)-2811	7300-1-T
b. PROJECT NO. 4161	
c. Task 416103	9b. OTHER REPORT NO(S) *(Any other numbers that may be assigned this report)*
d.	

10. AVAILABILITY/LIMITATION NOTICES

May obtain copies from DDC, Cameron Station, Alexandria, Virginia 22314

11. SUPPLEMENTARY NOTES	12. SPONSORING MILITARY ACTIVITY
	Air Force Avionics Laboratory, AVWC Research and Technology Division, AFSC Wright-Patterson Air Force Base, Ohio 45433

13. ABSTRACT

The transmission characteristics of an anisotropic panel formed by conducting discs are investigated theoretically in this work. The result is intended to interpret the characteristics of the loop loaded radant (radome-antenna) panel originally studied at the Air Force Avionics Laboratory. Experimental work on the impedance variation of a ferrite-loaded horn antenna in the presence of the panel and the radiation pattern of the antenna structure are also reported in this interim report.

DD FORM 1 JAN 64 1473

Unclassified

Security Classification

14. KEY WORDS	LINK A		LINK B		LINK C	
	ROLE	WT	ROLE	WT	ROLE	WT
Antennas Radomes						

INSTRUCTIONS

1. ORIGINATING ACTIVITY: Enter the name and address of the contractor, subcontractor, grantee, Department of Defense activity or other organization *(corporate author)* issuing the report.

2a. REPORT SECURITY CLASSIFICATION: Enter the overall security classification of the report. Indicate whether "Restricted Data" is included. Marking is to be in accordance with appropriate security regulations.

2b. GROUP: Automatic downgrading is specified in DoD Directive 5200.10 and Armed Forces Industrial Manual. Enter the group number. Also, when applicable, show that optional markings have been used for Group 3 and Group 4 as authorized.

3. REPORT TITLE: Enter the complete report title in all capital letters. Titles in all cases should be unclassified. If a meaningful title cannot be selected without classification, show title classification in all capitals in parenthesis immediately following the title.

4. DESCRIPTIVE NOTES: If appropriate, enter the type of report, e.g., interim, progress, summary, annual, or final. Give the inclusive dates when a specific reporting period is covered.

5. AUTHOR(S): Enter the name(s) of author(s) as shown on or in the report. Enter last name, first name, middle initial. If military, show rank and branch of service. The name of the principal author is an absolute minimum requirement.

6. REPORT DATE: Enter the date of the report as day, month, year; or month, year. If more than one date appears on the report, use date of publication.

7a. TOTAL NUMBER OF PAGES: The total page count should follow normal pagination procedures, i.e., enter the number of pages containing information.

7b. NUMBER OF REFERENCES: Enter the total number of references cited in the report.

8a. CONTRACT OR GRANT NUMBER: If appropriate, enter the applicable number of the contract or grant under which the report was written.

8b, 8c, & 8d. PROJECT NUMBER: Enter the appropriate military department identification, such as project number, subproject number, system numbers, task number, etc.

9a. ORIGINATOR'S REPORT NUMBER(S): Enter the official report number by which the document will be identified and controlled by the originating activity. This number must be unique to this report.

9b. OTHER REPORT NUMBER(S): If the report has been assigned any other report numbers *(either by the originator or by the sponsor)*, also enter this number(s).

10. AVAILABILITY/LIMITATION NOTICES: Enter any limitations on further dissemination of the report, other than those imposed by security classification, using standard statements such as:

(1) "Qualified requesters may obtain copies of this report from DDC."

(2) "Foreign announcement and dissemination of this report by DDC is not authorized."

(3) "U. S. Government agencies may obtain copies of this report directly from DDC. Other qualified DDC users shall request through

_____."

(4) "U. S. military agencies may obtain copies of this report directly from DDC. Other qualified users shall request through

_____."

(5) "All distribution of this report is controlled. Qualified DDC users shall request through

_____."

If the report has been furnished to the Office of Technical Services, Department of Commerce, for sale to the public, indicate this fact and enter the price, if known.

11. SUPPLEMENTARY NOTES: Use for additional explanatory notes.

12. SPONSORING MILITARY ACTIVITY: Enter the name of the departmental project office or laboratory sponsoring *(paying for)* the research and development. Include address.

13. ABSTRACT: Enter an abstract giving a brief and factual summary of the document indicative of the report, even though it may also appear elsewhere in the body of the technical report. If additional space is required, a continuation sheet shall be attached.

It is highly desirable that the abstract of classified reports be unclassified. Each paragraph of the abstract shall end with an indication of the military security classification of the information in the paragraph, represented as *(TS), (S), (C), or (U)*.

There is no limitation on the length of the abstract. However, the suggested length is from 150 to 225 words.

14. KEY WORDS: Key words are technically meaningful terms or short phrases that characterize a report and may be used as index entries for cataloging the report. Key words must be selected so that no security classification is required. Identifiers, such as equipment model designation, trade name, military project code name, geographic location, may be used as key words but will be followed by an indication of technical context. The assignment of links, rules, and weights is optional.